Predicting permeability from the characteristic relaxation time and intrinsic formation factor of complex conductivity spectra

A. Revil (1. 2, *), A. Binley (3), L. Mejus (3), and P. Kessouri (1)

1. Colorado School of Mines, Department of Geophysics, Green Center, 1500 Illinois Street, Golden, CO, USA
2. ISTerre, CNRS, UMR 5559, Université de Savoie, Equipe Volcan, Le Bourget du Lac, France
3. Lancaster Environment Centre, Lancaster University, Lancaster, UK.

(*) Corresponding author: André Revil (arevil@mines.edu)

Email addresses: arevil@mines.edu; kessouri@mines.edu; a.binley@lancaster.ac.uk; l.mejus@lancaster.ac.uk.

Key words: Complex conductivity, induced polarization, permeability, formation factor, relaxation time.

Intended for publication in Water Resources Research

Abstract. Low-frequency quadrature conductivity spectra of siliclastic materials exhibit typically a characteristic relaxation time, which either corresponds to the peak frequency of the phase or the quadrature conductivity or a typical corner frequency, at which the quadrature conductivity starts to decrease rapidly towards lower frequencies. This characteristic relaxation time can be combined with the (intrinsic) formation factor and a diffusion coefficient to predict the permeability to flow of porous materials at saturation. The intrinsic formation factor can either be determined at several salinities using an electrical conductivity model or at a single salinity using a relationship between the surface and quadrature conductivities. The diffusion coefficient entering into the relationship between the permeability, the characteristic relaxation time and the formation factor, takes only two distinct values for isothermal conditions. For pure silica, the diffusion coefficient of cations, like sodium or potassium, in the Stern layer is equal to the diffusion coefficient of these ions in the bulk pore water, indicating weak sorption of these couterions. For clayey materials and clean sands and sandstones whose surface have been exposed to alumina (possibly iron), the diffusion coefficient of the cations in the Stern layer appears to be 350 times smaller than the diffusion coefficient of the same cations in the pore water. These values are consistent with the values of the ionic mobilities used to determine the amplitude of the low and high-frequency quadrature conductivities and surface conductivity. The database used to test the model comprises a total of 202 samples. Our analysis reveals that permeability prediction with the proposed model is usually within an order of magnitude from the measured value above 0.1 mD. We also discuss the relationship between the different time constants that have been considered in previous works as characteristic relaxation time, including the mean relaxation time obtained from a Debye decomposition of the spectra and the Cole-Cole time constant.

1. Introduction

The complex conductivity of porous rocks is composed of an in-phase conductivity associated with the electromigration of ions in a porous material and a quadrature conductivity characterizing the ability of the porous material to store reversibly electrical charges [e.g., *Vinegar and Waxman*, 1984]). Such charge storage has been demonstrated to be related to the reversible polarization of the electrical double layer coating the surface of the grains [e.g., *Schwarz*, 1962; *Grosse*, 2009; *Vaudelet et al*., 2011a, b]. Complex conductivity can be imaged in the field using either galvanometric or induction-based methods [*Kemna et al*., 2004; *Karaoulis et al*., 2011; *MacLennan et al*., 2014]. Thanks to recent developments in introducing geological constraints or structural constraints from seismics and georadar in the tomography of DC resistivity [e.g., *Linde et al*., 2006; *Doetsch et al*., 2010; *Boucheda et al*. 2012; *Zhou et al*., 2014], complex conductivity can be now imaged in the field with an increasing level of accuracy and potentially used to image permeability with some confidence level that remains to be determined.

In the shallow subsurface (<100 m), the quest for permeability tomography remains one of the key drivers of hydrogeophysics given its control on groundwater flow and solute transport. Over the last three decades, a number of studies have shown that parameters derived from complex conductivity spectra can be used to predict directly permeability [for instance *Slater and Lesmes*, 2002; *Binley et al*., 2005; *Revil and Florsch*, 2010; *Titov et al*., 2010; *Koch et al*., 2011, 2012]. Some other works have shown that complex conductivity spectra are sensitive to some textural parameters controlling permeability such as the main pore-throat size [*Scott and Barker*, 2003], the pore size distribution [*Revil et al*., 2014a], or the surface area per pore volume ratio [*Kruschwitz et al*., 2010].

Models describing the relationships between the complex conductivity and the permeability fall into two categories. The first set of models exploits either the magnitude of the quadrature conductivity (or normalized chargeability) and the formation factor [e.g.,

Börner et al., 1996; Worthington and Collar, 1984; *Revil and Florsch*, 2010; *Weller et al*., 2015b]. The second set of models use a relaxation time extracted by some means from the spectra, which is assumed to be characteristic of the hydraulically effective length scale [e.g., *Pape and Vogelsang*, 1996; *Binley et al*. 2005; *Revil et al*., 2012]. Our approach, in this paper, belongs to this second category.

Our goal is to test further the petrophysical model developed recently by *Revil et al.* [2012] based on the peak frequency of the phase or quadrature conductivity and the intrinsic formation factor (i.e., corrected for surface conductivity). We test this model on a broader database than used so far and we develop a complete methodology to determine permabiity from induced polarization tomography. The database used in the current study includes 4 datasets with a total of 202 core samples including a total of 40 new samples. Dataset #1 corresponds to a total of 22 clean sands and sandstones. Dataset #2 includes essentially 36 sandstones and low-porosity Fontainebleau sandstones (porosity below 0.16). Dataset #3 corresponds to 18 sandstones. The complex conductivity spectra of the core samples belonging to datasets #1 to #3 have been obtained in the frequency domain. Dataset #4 corresponds to the 123 sandstones from the database of *Tong et al.* [2006a] measured in the time domain. Since in the above-mentioned studies different relaxation time parameters were considered as a characteristic relaxation time for permeability estimation, we also analyze the general relationships between these parameters for a typical spectral response with Cole-Cole type behavior.

2. Background

We first review the fundamental equation developed by *Revil et al.* [2012] to determine the permeability using a characteristic frequency (such as the peak frequency) and the intrinsic formation factor and then discuss its assumptions.

2.1. The characteristic relaxation time of polarization

The complex electrical conductivity of a porous rock, $\sigma^*(\omega)$, is expressed as

$$\sigma^*(\omega) = |\sigma(\omega)| \exp\left(i\varphi(\omega)\right), \tag{1}$$

where ω is the angular frequency (rad s^{-1}), $i = \sqrt{-1}$ the pure imaginary number, $\varphi(\omega)$ (rad) denotes the phase lag between the current and the voltage, and $|\sigma(\omega)|$ (S m^{-1}) the amplitude of the conductivity. To account for the amplitude of the conductivity and the phase, the conductivity can be written as a complex number

$$\sigma^*(\omega) = \sigma'(\omega) + i\sigma''(\omega), \tag{2}$$

where $\sigma'(\omega)$ ($\geq$0) and $\sigma''(\omega)$ ($\leq$0) denote the in-phase and quadrature components of the complex conductivity, respectively. This convention is from *Fuller and Ward* [1970] and *Keller* [1988]. Note that some authors use another convention with $\sigma^*(\omega) = \sigma'(\omega) - i\sigma''(\omega)$ and therefore $\sigma''(\omega)$ is positive. Further information regarding the experimental procedure and the experimental apparatus used to obtain spectra in frequency-domain induced polarization can be found in *Vinegar and Waxman* [1984], *Zimmerman et al*. [2008a, b], *Revil and Skold* [2011], and *Okay et al*. [2014].

In this paper, we base our analysis on three observations made by Revil and co-workers in their recent papers [*Revil et al*., 2012; *Revil*, 2013a, b; *Revil et al*., 2014a]:

(1) Low-frequency quadrature conductivity spectra usually exhibit one of two types of behavior, each of them characterized by their own characteristic frequency (see discussion in *Revil* [2013b] and Figure 1) and thus relaxation time. These two behaviors can be observed in the spectra displayed in Figures 1 to 6. Type A (Figure 1) corresponds to spectra showing a well-defined frequency peak. The clayey sandstones of Figures 3a and 6, the St Bees sandstones of Figure 4, and the Saprolite core sample and the sand of Figure 5 all exhibit a well-defined frequency peak. In this case, we can pick the peak frequency (using, for example, a polynomial function), f_p, and relate it to a peak relaxation time $\tau_p = 1/(2\pi f_p)$. There is another family of spectra displaying a characteristic "corner" frequency, f_c, at which the

quadrature conductivity starts to decrease rapidly towards lower frequencies (Type B, Figure 1), again related to a relaxation time $\tau_c = 1/(2\pi f_c)$. Figure 3 shows such type of spectrum for the Berea sandstone. In this second case, we can fit a linear function to the low-frequency decay and the plateau and we look for the intersection between the two lines in a log-log plot. There are exceptions to this rule especially for rocks such as tight oil and gas shales for which the strength of the phase (or quadrature conductivity) continuously increase with the frequency [*Revil et al*., 2013b; *Woodruff et al*. 2014]. This is especially the case for porous materials characterized by small pore sizes associated therefore to a high-frequency induced polarization, which overlaps with the Maxwell-Wagner polarization. Some authors have also reported flat spectra over a narrow range of frequencies [*Vinegar and Waxman*, 1984]. Since however the physics of induced polarization dictates that the quadrature conductivity and the phase need to go to zero at zero frequencies (as implied by the Kramers Kronig relationships of causality), it implies that these authors did not investigate frequencies that were low enough to see the corner frequency mentioned in the Type B spectra above.

(2) The distribution of relaxation times is obtained through a deconvolution with an appropriate relaxation model describing the polarization response of an individual pore [e.g., *Titov et al.*, 2002]. Therefore the distribution of relaxation times is closely related to the pore size distribution, which can be determined to some extent by the capillary pressure curve [e.g., *Revil et al*., 2014a]. The idea that the distribution of relaxation times and the pore size distribution are connected can be found in the works of, for example, *Vinegar and Waxman* [1988] and *Tong et al*. [2006a]. In recent studies, the decomposition has been performed on the basis of the Debye relaxation model, and frequently the geometric mean value of the resultant Debye relaxation time distribution, τ_{mD}, is considered as a characteristic relaxation time [e.g., *Tong et al.*, 2006a; *Nordsiek and Weller*, 2008]. However, other definitions of a characteristic relaxation time have also been used [e.g., *Zisser et al.*, 2010], and the most

appropriate choice still remains unclear. For Type B, the corner frequency may correspond to the largest pores controlling permeability.

(3) Models predict a characteristic relaxation time, τ_0, which is associated with a characteristic pore size Λ according to [*Revil et al*., 2012]

$$\tau_0 = \frac{\Lambda^2}{2D_{(+)}}, \tag{3}$$

where $D_{(+)}$ denotes the diffusion coefficient of the counterions in the Stern layer, the inner part of the electrical double layer. In Equation (3), Λ is considered to be the length scale used by *Avellaneda and Torquato* [1991] and the numerical constant is somewhat arbitrary (see *Revil* [2013a] for details). Equation (3) implies that the characteristic relaxation time is expected to be poorly dependent on the salinity, which is indeed supported by a number of experimental data (as shown, for example, in the spectra analyzed in Figure 5, for both a clayey saprolite and a clean sand). For our analysis, we assume that, depending on the observed spectral behavior (Type A or Type B), the relaxation times τ_p or τ_c, respectively, are representative values for the relaxation time τ_0, which is related to the characteristic length scale according to Equation (3). *Klein and Sill* [1982] show that increasing clay content in a mixture with glass beads is responsible for an increase of the time constant τ_0. As discussed below in Section 2.3, this experimental result is consistent with Eq. (3) since despite the reduction of the pore size, there is a strong reduction of the diffusion coefficient for clays by comparison with (pure) silica beads. Note that depending on the local radius of curvature of the interface between the solid phase and the pore space, it is possible that the relaxation time can be associated with the grain size for colloids. This matter still needs to be investigated in detail.

2.2. Connection to permeability

The permeability is related to the pore length Λ by [*Avellaneda and Torquato*, 1991]

$$k = \frac{\Lambda^2}{8F}, \tag{4}$$

where F denotes the intrinsic formation factor of the material (dimensionless). From Equations (3) and (4), the permeability can be determined from the characteristic relaxation time τ_0 and the intrinsic formation factor F according to,

$$k = \frac{D_{(+)}\tau_0}{4F}. \tag{5}$$

This equation is the key equation used in this paper. *Johnson et al*. [1986] noted that the ratio $8Fk/\Lambda^2$ in fact tends to be between 1.4 and 2.5 (although this was based on a small dataset). Therefore, the factor 4 in Eq. (5) can be questionable.

According to equation (5), the formation factor and the characteristic relaxation time are equally important in defining the permeability of the porous medium. *Tong et al.* [2006a] observed that using the (intrinsic) formation factor rather than the connected porosity alone improves the predictive capabilities of the formula used to predict permeability from the relaxation time. In the laboratory, the formation factor can be determined using the in-phase conductivity alone. However, such determination requires doing conductivity measurements at least at two salinities [*Vinegar and Waxman*, 1984]). Some authors determine their formation factor using a single high salinity measurement. While this methodology is generally fine for most core samples, care should be taken for materials characterized by a high surface conductivity. Indeed, there is no guarantee that the effect of surface conductivity is negligible at high salinities, especially for smectite–rich materials [*Bernabé and Revil*, 1995].

Recent works indicate that the intrinsic formation factor can be also determined from the complex conductivity measured at a single salinity using a new relationship between the surface and quadrature conductivities (for details, see *Revil* [2013a], *Weller et al.* [2013], and *Revil* [2014]). Note that equation (5) exhibits some similarities to the empirical equation

found by *Tong et al*. [2006a] for their experimental data set: $k = 6.0\times10^{-14}\tau_0^{1.60}F^{-0.81}$ (where k is in m^2 and τ_0 in s, and where the geometric mean Debye relaxation time is taken for τ_0).

2.3. The diffusion coefficient

According to *van Olphen and Waxman* [1958], clay minerals are characterized by a compact electrical double layer coating the grains with a high fraction of the counterions strongly sorbed on the mineral surface. They claim that the ions of the Stern layer (the inner part of this electrical double layer) of clay minerals have a mobility much smaller than in the diffuse layer and the bulk pore water. *van Olphen and Waxman* [1958] stated that silica have, in contrast, a well-developed diffuse layer with no indication of specific adsorption forces between surface and counter ions. *Carroll et al*. [2002] showed that the surface of silica in contact with a NaCl solution possesses a Stern layer of very weakly sorbed counterions characterized by weak sorption of counterions like sodium. This indicates that the mobility of such counterions in the Stern layer of silica is probably the same as in water [*Carroll et al*., 2002]. We will advocate also, below, that a small amount of alumina can change drastically the properties of the surface of silica and we will divide the data into pure silica and clayey sands, this distinction being entirely based on the electrochemical properties of mineral surfaces.

The value of the diffusion coefficient $D_{(+)}$ entering our model is related to the mobility of the counterions in the Stern layer, $\beta^S_{(+)}$, by the Nernst-Einstein relationship $D^S_{(+)} = k_b T \beta^S_{(+)} / \left|q_{(+)}\right|$, where T denotes the absolute temperature (in K), k_b denotes the Boltzmann constant (1.3806×10^{-23} m^2 kg s^{-2} K^{-1}), $\left|q_{(+)}\right|$ is the charge of the counterions in the Stern layer coating the surface of the grains. For clays, $\beta^S_{(+)}$ (Na^+, 25°C) = 1.5×10^{-10} $m^2s^{-1}V^{-1}$ yields $D_{(+)}$ (Na^+, 25°C) = 3.8×10^{-12} m^2s^{-1} (see *Revil* [2012, 2013a, b]). For clean sands and sandstones, the mobility of the cations in water leads to a diffusion coefficient of $D_{(+)}$ (Na^+,

25°C) = 1.3×10^{-9} m^2s^{-1}. Thus, the concept that there are two values for the mobility of the counterions implies in turn that there are two discrete values for their diffusion coefficients, one for clean sands (pure silicates) and one for aluminosilicates (clays) and silicates contaminated with alumina. Accordingly, Equation (5) can be used with $D_{(+)}$ = 3.8×10^{-12} m^2 s^{-1} at 25 °C for clayey sandstones and $D_{(+)}$ = 1.3×10^{-9} m^2 s^{-1} at 25 °C for clean sandstones with clean silica surfaces (see *Revil* [2012] for an extensive discussion of this point). We will discuss again this point at the end of the paper but the readers are directed to *Revil* [2014] for further discussion and *Weller et al.* [2015a] for a contrasting opinion based on a new set of experimental data.

In the case of Fontainebleau sandstones, *Revil et al.* (2014b) pointed out that despite the fact that the Fontainebleau sandstone is a clean sandstone (99.8% silica), its surface properties are not those of pure silica. They explained that the silica cement of the Fontainebleau sandstone possess a number of impurities (Fe, Al) modifying its interfacial properties [*Chappex and Scrivener*, 2012]. This is consistent with our findings (shown later) that low-porosity Fontainebleau sandstones have properties similar to clayey materials while high-porosity Fontainebleau sandstones have properties similar to pure silica. Therefore for natural sandstones, if the surface of the grains is contaminated by alumina and iron, it is possible that their surface will exhibit a behavior closer to the surface of clayey materials. Figure 7 shows that alumina can be easily incorporated into silica and transform the properties of the mineral surface in creating aluminol and silanol surface sites like in clays [*Iler*, 1979]. The strong affinity of alumina for the surface of silica and its drastic effect on the electrical double layer properties has been broadly recognized in the literature [*Ishido and Mizutani*, 1981]. In our case, it means that the distinction that should be done between a “clayey sand behavior” and a “clean sand” behavior is not controlled by the amount of clays in the materials but by the properties of the mineral surface since a small amount of alumina can

strongly affect the properties of the mineral surface. This assertion will need, however, to be further backup by new experimental checks in the future and spectroscopic analysis of the mineral surfaces.

2.4. Frequency versus time domain measurements

Complex conductivity measurements can be performed in the time or frequency domain. There are several ways to determine a characteristic relaxation time in time and frequency domains using a variety of tools such as the Debye decomposition technique [*Nordsiek and Weller*, 2008], as already outlined in Section 2.1. To illustrate the correspondence between frequency- and time-domain measurements, we consider the Cole-Cole model as an example of the spectral response, since often a response similar to a Cole-Cole model response is observed. In this case, the complex conductivity in the frequency-domain is written as:

$$\sigma^*(\omega) = \sigma_\infty \left[1 - \frac{M}{1 + \left(i\omega\tau_{CC} \right)^c} \right], \tag{6}$$

where τ_{CC} is the Cole-Cole time constant, c is the Cole-Cole exponent, $M = (\sigma_\infty - \sigma_0)/\sigma_\infty$ is the dimensionless chargeability, σ_0 and σ_∞ denoting the DC (ω=0) and high-frequency electrical conductivities, respectively.

In the time domain, and still adopting a Cole-Cole model, and assuming the primary current has been injected for a sufficient long time (so all the polarization length scales are fully polarized), the voltage decay is given by [e.g., *Florsch et al*., 2011]

$$\psi(t) = \psi_1 \sum_{j=0}^{\infty} \frac{(-1)\left(\frac{t}{\tau_{CC}} \right)^{jc}}{\Gamma(1 + jc)}, \tag{7}$$

where j denotes here the summation index, ψ_1 denotes the secondary voltage just after the shutdown of the primary current, and Γ is Euler's Gamma function defined by

$$\Gamma(x) = \int_0^\infty u^{x-1} e^{-u} du \,. \tag{8}$$

The secondary voltage is related to the chargeability M and the primary voltage ψ_0 (existing in steady-state conditions during the injection of the electrical current) by

$$M = \frac{\psi_1}{\psi_0}. \tag{9}$$

Therefore the voltage decay is given by,

$$\psi(t) = \psi_0 M \sum_{j=0}^{\infty} \frac{(-1)\left(\frac{t}{\tau_{CC}}\right)^{jc}}{\Gamma(1+jc)}. \tag{10}$$

Therefore, fitting data using a time-domain function like the Cole-Cole model can be used to determine a relaxation time, here the Cole-Cole time constant τ_{CC}. It should be noted, however, that this procedure is formally correct only if the primary current has been imposed long enough to the porous rock, so that all the polarizable elements, including the largest, have been polarized. This corresponds typically to over 100 s according to *Tong et al*. [2006a]. If this is not the case, the relaxation time obtained through time-domain induced polarization measurements can be inadequate for estimating permeability.

If time domain induced polarization data are used, one needs also to care of using four electrodes and to avoid using the data for the first 400 ms after the shut-down of the primary current (since they contain Maxwell-Wagner and possibly electromagnetic coupling effects). *Ghorbani et al.* [2007] developed some strategies to accurately determine the Cole Cole relaxation time from both time-domain and frequency-domain induced polarization measurements. In addition, the Cole Cole model can be applied even if the spectra are not perfectly symmetric as discussed in details by *Revil et al*. [2014a]. The spectra only need to be symmetric close to the relaxation peak.

2.5. Condition of validity of Equation (5)

There are several assumptions under which the relationship between the characteristic relaxation time, the formation factor, and the permeability, may be invalid. An obvious case is when the rock hosts semi-conductors such as pyrite or magnetite. In this case, a polarization with usually a clear and relatively strong phase peak can be associated with the presence of these minerals. This polarization has nothing to do with the pore sizes and therefore with the permeability of the porous material but strongly dominates the quadrature (or phase) spectra (e.g., *Wong* [1979]). The second case, which is much less trivial, is related to the way the clay minerals are located in the pore space of the sandstone. Four cases can be considered and are illustrated in Figure 8. Equation (5) is likely to be valid for the case of clean sandstones since the polarization length scale is expected to be controlled by the grain or pore sizes. The case of clayey sandstones is less obvious. If the clay minerals are dispersed in the porous material (e.g., coating the sand grains), Equation (5) is still expected to perform well. However, in the structural or laminar shale cases (see Figure 8), the polarization length scale(s) associated with the polarization of the porous material can be totally disconnected from the relevant length scale(s) needed to determine permeability.

2.6. Uncertainty regarding the relaxation time

The uncertainty in the determination of the relaxation time is an important issue to estimate the resulting uncertainty in the predicted permeability. In practice, however, this is extremely challenging. The three repeat measurements used to determine the standard deviation for each data point in our laboratory are not very suitable for this purpose. The uncertainty cannot be therefore consistently assessed for all datasets used in this study. The Bayesian uncertainty analysis of relaxation time discussed in *Koch et al.* [2012] is not really appropriate either because it assumes that the spectra can be described by an analytical model such a Cole-Cole response. The obtained uncertainty in the relaxation time strongly depends on the adequacy of this assumption, which is difficult to estimate. Therefore, in this paper,

while we recognize that the determination of the uncertainty if the relaxation time is an important issue but we will not try to assess a general methodology to assess this uncertainty.

3. Relationship between different relaxation time parameters

Using equation (5) for permeability estimation requires inferring the characteristic relaxation time, τ_0, from the measured an induced polarization spectrum. As outlined in Section 2.1, different relaxation time parameters have been considered as characteristic relaxation times in previous works, including peak relaxation time, τ_p, the corner relaxation time τ_c, Cole-Cole relaxation time, τ_{CC}, and some sort of relaxation time derived from a Debye decomposition, here mainly the geometric mean value, τ_{mD}, of the resultant relaxation time distribution [e.g., *Tong et al.*, 2006a; *Nordsiek and Weller*, 2008; *Zisser et al.*, 2010]. Obviously all these relaxation time parameters, for a general shape of the spectrum, differ to some degree. A direct comparison of characteristic relaxation times reported in the literature is further complicated by the fact that they can be determined based on the complex conductivity spectrum or the complex resistivity spectrum, or – in the case of τ_p – based on the phase spectrum or the imaginary spectrum, all providing different results [*Florsch et al.*, 2012; *Tarasov and Titov*, 2013]. Even for a perfect Cole-Cole model response, τ_{CC} and τ_p become equal only if the chargeability M approaches zero (based on a complex resistivity parameterization, it is $\tau_{CC} = \tau_p\,(1-M)^{1/2c}$) [e.g., *Tarasov and Titov*, 2013], and τ_{CC} and τ_{mD} are only equal if the parameterization of the log relaxation time distribution underlying the Debye decomposition symmetrically covers the peak in the spectrum. The latter is an obvious result when recalling that the Cole-Cole model response can be described by a superposition of Debye model responses for a symmetric log distribution of relaxation times [e.g., *Cole and Cole*, 1941].

We can also comment on the use of the Debye model as kernel for the decomposition of the spectra. A problem with this choice was highlighted recently by *Revil et al.* [2014a].

There is no evidence that the Debye model response appropriately represents the elementary polarization response of a single pore or length scale in a rock. For example, the short-narrow-pore model by *Titov et al.* [2002] predicts a Cole-Cole type response with c = 0.62, a value which *Tarasov et al.* [2003] also used in their decomposition procedure. *Revil et al* [2014a] argued that in the decomposition the Debye model response should be replaced by a Warburg model response (i.e., a Cole-Cole type response with c = 0.5) to obtain a more appropriate distribution of relaxation times. Note that *Florsch et al.* [2014] offered recently a more general framework to decompose spectra using different types of response functions.

4. The Intrinsic Formation Factor

A very important ingredient of our approach is a reliable measurement of the intrinsic formation factor, since the "apparent" formation factor (ratio of the conductivity of the pore water by the conductivity of the material) is not a textural property of the pore network and would lead to an overestimation of the permeability if used in Eq. (5). When the conductivity of the rock sample is obtained at several salinities, there are well-established methods to fit the conductivity equation to get the intrinsic formation factor [e.g., *Vinegar and Waxman*, 1984]. The problem is when the complex conductivity data are obtained at a single salinity, including a high salinity (for cases where significant surface conductivity exists). If the porosity is available, and a value of the cementation exponent can be estimated from the cation exchange capacity and the porosity of the core sample [*Revil et al.*, 1998, their Figure 5], the formation factor can be obtained through Archie's law. Another way is to use a recently developed relationship between the quadrature conductivity and the surface conductivity to estimate the intrinsic formation factor. These approaches are discussed in the next sections.

4.1. Tests of Archie's law

In a number of papers in hydrogeophysics, authors do not make the distinction between intrinsic and apparent formation factors. The apparent formation factor is defined as the ratio between the low salinity pore water conductivity divided by the conductivity of the core sample. However, even for a clean sandstone like the Fontainebleau sandstone, *Revil et al.* [2014b] showed recently that there is a substantial difference between the intrinsic and apparent formation factors at low salinities, typically for what is considered fresh water (Figure 9). It is clear that if we consider the apparent formation factor instead of the intrinsic one, we cannot achieve an accurate estimate of the permeability, which will be overestimated since the apparent formation factor is always smaller than the intrinsic formation factor.

We test here the validity of Archie's law $F = \phi^{-m}$ that can be used to estimate the intrinsic formation factor from the porosity. In Figure 10, we use the data from Tables 1 from *Revil et al*. [2014b] and the data from the database described in Section 5. We see that for the clean and clayey sandstones, we can fit the data with Archie's law with a single prescribed value of the cementation exponent *m*. Usually, we expect that the value of the cementation exponent will also increase slightly with the cation exchange capacity of the material, so with the clay content at a given clay mineralogy, as explained by *Revil et al.* [1998] (their Figure 5).

Among the references used to build our database, there are cases for which the provided values of the formation factor do not seem reliable. For instance in *Titov et al.* [2010], the provided value of the formation factor of the Portland sandstone yields a cementation exponent smaller than 1, which is physically impossible (see Appendix A in *Revil* [2013a], equation A15). In this case, we used Archie's law to determine the value of the formation factor. This will be the case for the value provided by *Titov et al*. [2010] for the Portland sandstone and for the dataset from *Tong et al.* [2006a] (full dataset #4).

4.2. Using the Quadrature Conductivity

Usually, the frequency dependence of the in-phase conductivity is weak (i.e., the chargeability is much smaller than one) and can be, at first approximation, neglected. With this assumption, the (in-phase) conductivity can be written as (see Appendix A),

$$\sigma' \approx \sigma_\infty = \frac{1}{F}\sigma_w + \sigma_S\,, \tag{11}$$

where σ_S is called surface conductivity and is determined by (Appendix A),

$$\sigma_S = \left(\frac{1}{F\phi}\right)\rho_S\left[\beta_{(+)}(1-f) + \beta^S_{(+)} f\right]\mathrm{CEC}\,, \tag{12}$$

When the above assumption is not valid, for instance at very low salinities or for a very high volume fraction of clay minerals with a high cation exchange capacity, the in-phase conductivity should be simply replaced by its high-frequency asymptotic limit σ_∞ in the equations derived below. As seen above, the quadrature conductivity can be determined around the peak frequency as,

$$\sigma'' \approx -\frac{M_n}{5} \tag{13}$$

$$M_n = \left(\frac{1}{F\phi}\right)\rho_S \beta^S_{(+)} f\ \mathrm{CEC}\,. \tag{14}$$

Revil [2013b] introduced a dimensionless ratio R between the quadrature conductivity or normalized chargeability and the surface conductivity. In the present paper, we use the following definition for the dimensionless number R:

$$\mathrm{R} \equiv \frac{M_n}{\sigma_S} \approx -5\left(\frac{\sigma''}{\sigma_S}\right). \tag{15}$$

Using Eqs. (12) and (14), R can be related to the partition coefficient *f*,

$$\mathrm{R} = \frac{\beta^S_{(+)} f}{\left[\beta_{(+)}(1-f) + \beta^S_{(+)} f\right]}\,. \tag{16}$$

Equation (16) will however not be used further below. We can analyze the value of R for sands and clays. Using a broad database of core samples, *Weller et al.* [2013] obtained for the ratio between quadrature and surface conductivity $-\sigma''/\sigma_S$ = 0.042 (using data fitting). In Figure 11, the database consists of data from *Weller et al.* [2013] (sands and sandstones), *Woodruff et al.* [2014] (tight oil and gas shales) and *Revil et al.* [2014b] (clean Fontainebleau

sandstone covering a broad porosity range). This dataset allows testing the predicted linear relationship between the quadrature conductivity and the surface conductivity over 6 orders of magnitude. The plain line in Figure 11 is consistent with $-\sigma''/\sigma_S$ = 0.042.

Using a broad database of core samples, *Weller et al*. [2013] obtained (using data fitting) R = 0.20 for the ratio between normalized chargeability and surface conductivity (see Figure 12 with the addition of the dataset given in Table 1 extending the trend to higher and lower normalized chargeabilities). Therefore, the value determined in Figure 11 is in excellent agreement with the present model. Indeed, according to Equation (15), a ratio of $-\sigma''/\sigma_S$ = 0.042 yields R = 0.21 close to the value given above. Equation (15) seems therefore very robust. This also is true in unsaturated conditions and in anisotropic materials such as oil and gas shales as discussed by *Woodruff et al*. [2014].

We can therefore now determine the formation factor using the in-phase and quadrature conductivities at a single frequency. Equations (11) and (15) yield a new petrophysical relationship:

$$\sigma' \approx \frac{1}{F}\sigma_w - \frac{5\sigma''}{R}, \tag{17}$$

Börner et al. [1996], *Weller et al*. [2013], and *Revil* [2013b] have developed a method to estimate the intrinsic formation factor from the knowledge of the pore water conductivity and the in-phase and quadrature conductivities. In the context of our model, Eq. (17) yields

$$F = \frac{\sigma_w}{\sigma' + \frac{5\sigma''}{R}}, \tag{18}$$

where the quadrature conductivity is taken as a negative number. Equation (18) can be used to image, at the field scale, the intrinsic formation factor knowing the conductivity of the pore water σ_w and images of the in-phase and quadrature conductivities. Note that the formation factor is strictly independent of the frequency. However, because we have neglected the

frequency dependence of the in-phase conductivity, it may appear slightly dependent on the frequency if Eq. (18) is used with the assumption stated above.

5. Database

In this section, we describe the four datasets used in our analysis. For each dataset, we describe the way the data were acquired (equipment and time-domain versus frequency-domain measurements), the composition of the pore water, and the way the porosity and permeability were obtained.

5.1. Dataset #1

This dataset (Table 1) includes a total of 22 clean sands and the high-porosity Fontainebleau sandstones. We measured the complex conductivity spectra of 3 Fontainebleau sandstones. The experimental procedure is described in *Revil et al*. [2014b] and will not be repeated here (some of these spectra are shown in Figure 2). These three core samples with the highest porosity exhibit quadrature conductivity properties that are consistent with clean sands in terms of the value of $D_{(+)}$ needed to fit the data. In contrast and consistently with *Revil et al*. [2014b], the reported permeability are gas permeability corrected for the Klinkenberg effect (see discussion in *Revil et al*. [2014b] for a presentation of the dataset and see *Klinkenberg* [1941], for a description of this correction). The pore water was obtained by mixing distilled water and pure NaCl to control the salinity and NaOH to control the pH. We used a conductivity of 165 μS cm^{-1} and a pH of 7.2.

In Dataset #1, we also use the experimental data from *Koch et al*. [2011, 2012] who investigated clean sands with interfacial properties consistent with the properties of pure silica. All the samples from *Koch et al*. [2011, 2012] were considered with the exception of sample SP3, which contains plate-like particles of mica with a length of approximately one millimeter (see *Revil et al*. [2013a]) and which behaves anomalously with respect to the complete dataset. The permeability to water was measured with a permeameter in steady-state

flow conditions. For the complex conductivity measurements, the samples were saturated with a NaCl electrolyte with an electrical conductivity σ_w ranging from 40 to 60 μS cm^{-1} (at 25°C).

Finally this datasets also includes measurements on four sands from four studies. For the New-Zealand sand investigated by *Joseph et al*. [2015], the conductivity of the pore water varied between 12 to 900 μS cm^{-1} (at 25°C, KCl). The frequency band investigated was 0.01 Hz to 1 kHz using a custom-built impedance meter. The permeability to water was determined with a constant head method. The sand U30 investigated by *Revil and Skold* [2011] was saturated by a NaCl solution (10 mM, pH 6.75) under vacuum. Electrical conductivity spectra were measured at 19 frequencies over the frequency range 2 mHz - 45 kHz using the ZEL-SIP04-V02 impedance spectrometer (Forschungszentrum Julich GmbH) [*Zimmermann et al*., 2007]. Sample Bu12 ("Bunter Sandstone") was investigated by *Weller et al.* [2011] using NaCl solutions (960 to 21880 μS cm^{-1}, 20°C). The complex conductivity was acquired over a frequency range 2.8 mHz - 12 kHz using a Fuchs impedance meter. Porosity was determined by the standard triple weight technique. Though no clay minerals were identified by microscope in this sample, a considerable amount of hematite causes its reddish color (A. Weller, personal communication, 2015). Iron oxides like hematite have, however, a very small induced polarization signature [*Aal et al*., 2014] that we consider negligible here when the hematite is present in small quantities.

5.2. Dataset #2

This dataset (Table 2) comprises a total of 36 samples (mostly sandstones) including 11 low-porosity Fontainebleau sandstones showing polarization data consistent with clayey sandstones. The procedure used to investigate these 12 Fontainebleau sandstone samples is the same as reported above in Section 4.1.

We have also added 6 samples from the study of *Revil et al.* [2014a], 5 clayey sandstones and one mudstone. Permeability was estimated using the capillary entry pressure curve with a resolution better than half an order of magnitude (see *Revil et al.* [2014a] for a complete description of the methodology). For the complex conductivity measurements, these samples were saturated with a natural groundwater with a TDS (Total Dissolved Solids) of 318 mg L^{-1}, a pH of 8.1, and an electrical conductivity σ_w (at 25°C) of 479 μS cm^{-1}. The main cations and anions of the natural pore water were Na^+ (30.6 mg L^{-1}), Ca^{2+} (65 mg L^{-1}), K^+ (3.9 mg L^{-1}), Cl^{-1} (6.0 mg L^{-1}), HCO_3^- (123 mg L^{-1}) and SO_4^{2-} (132 mg L^{-1}), and an alkalinity of 109 mg L^{-1}). Their spectra are shown in Figure 3.

Dataset #2 contains three Berea sandstones with characteristic relaxation time in the range 2 - 8 s. This can be compared with the value of 1.3 s inverted by *Keery et al.* [2012] using a Cole Cole model and the value of 1.8 s reported in Table 3 from the peak frequency of the same dataset. The Berea sandstones investigated by *Lesmes and Fry* [2001] and *Lesmes and Morgan* [2001] was saturated with a KCl solution at 0.01 M. Porosity and permeability were determined using a helium porosimeter and a nitrogen permeameter. The two Berea sandstones investigated by *Titov et al*. [2010] were saturated with two distinct NaCl solutions at 5 S m^{-1} and 0.2 S m^{-1} (25°C). Their permeability was determined using a gas permeameter.

We also measured one sample from the Portland formation, the same formation that was investigated by *Titov et al.* [2010] using time domain measurements. The reason for this new test was that the results obtained by *Titov et al.* [2010] for their Portland sample were inconsistent with the model tested in the present work. We wanted to check if this sandstone was a special case for which the present model would not apply (see Figure 8). The investigated sample (Sample PS1, Table 2) is characterized by a permeability to water of 0.1 mD for a porosity of 0.194, and a grain density of 2666 kg m^{-3}. We performed spectral induced polarization measurements on this core sample (Figure 6). The pH of the saturating fluid was 9.1 and the conductivity of the pore water was 1.70×10^{-2} S m^{-1} (NaCl). The Portland

formation is characterized by a very high clay content with mostly kaolinite and illite (Table 3). The normalized chargeability $M_n = M\sigma_\infty = \sigma_\infty - \sigma_0$ was determined from the in-phase conductivity spectrum (used to determine σ_∞ and σ_0) to be 4±1×10^{-3} S m^{-1}. Using $\mathrm{R} = M_n / \sigma_S \approx 0.2$ (see *Weller et al*. [2013] and Section 4.2 above), we obtain a surface conductivity $\sigma_S \approx 2\times10^{-2}$ S m^{-1}. The surface conductivity determined from the conductivity data shown in Figure 9b is $\sigma_S \approx 2.4\times10^{-2}$ S m^{-1}, therefore, in close agreement. Since the intrinsic formation factor is close to 44 (Figure 9b), this indicates that at low salinity, most of the conductivity response of the Portland formation is controlled by the surface conductivity. The discrepancy between our results and the results of *Titov et al*. [2010] could be explained because the two core samples, despite coming from the same formation, are vastly different with one having for instance some microcracks (K. Titov, personal communication, 2015). Another explanation could be that the approach used by *Titov et al*. [2010] of using a Cole Cole model to interpret their time-domain induced polarization data is not valid because the spectrum of the Portland sample displays a very asymmetric shape (A. Weller, personal communication, 2015).

The dataset also contains one saprolite core sample from *Revil et al.* [2013a] and five other sandstones from the study of *Titov et al.* [2010]. The saprolite core sample was investigated with a NaCl solution (300 mM). Complex conductivity was measured over the range of 1 mHz to 45 kHz using the ZEL-SIP04-V02 impedance spectrometer (Forschungszentrum Julich GmbH) [*Zimmermann et al*., 2007] (see Figure 5a). Its permeability was measured in a water permeameter whereas its porosity was determined using the Archimedes method (triple weight measurements). The five sandstones investigated by *Titov et al*. [2010] were saturated with two distinct NaCl solutions (4.31 S m^{-1} and 5.9×10^{-2} S m^{-1}, at 25°C). Their permeability was determined using a gas permeameter.

Finally, we also considered 7 samples from the Triassic St Bees formation (part of the Sherwood Sandstone Group). The St Bees sandstone is a red-brown, very fine- to medium-grained, commonly micaceous sandstone [*Allen et al*., 1997]. The 25 mm diameter, 40 mm long plug samples were obtained from sections of a 100 m diameter core covering an interval of 17 m, drilled in the Eden valley, Cumbria, UK. Porosity of the samples was measured gravimetrically using de-aired water under vacuum. Gas permeability was measured at the hydrogeological properties laboratory at British Geological Survey (Wallingford, UK) and a Klinkenberg correction was applied. The permeability range was 366 mD to 0.71 mD. In order to measure electrical properties, the samples were saturated under vacuum at four different salinities (NaCl): 5 mM, 0.01 M, 0.1 M, and 0.5 M. Once saturated at each salinity, samples were left to equilibrate for at least 24 hours before measurements were made. For all samples, the complex conductivity was measured at 19 frequencies over the range of 2 mHz to 45 kHz using the ZEL-SIP04-V02 impedance spectrometer (Forschungszentrum Julich GmbH) [*Zimmermann et al*., 2007]. The sample holder described in *Binley et al*. [2005] was used for electrical measurements.

5.3. Dataset #3

Dataset #3 (Table 4) comprises a total of 18 core samples of clayey sandstones from a range of sources. Induced polarization measurements were made in the frequency domain on samples saturated with a 0.01M NaCl solution. The formation factors were determined at high salinity (1 M NaCl) saturation, i.e. it was assumed that surface conductivity at this salinity was negligible. Porosity of the samples was measured gravimetrically using de-aired water under vacuum. Gas permeability was measured at the hydrogeological properties laboratory at British Geological Survey (Wallingford, UK) and a Klinkenberg correction was applied. For all samples, complex conductivity spectra were measured at 19 frequencies over the range 2 mHz - 45 kHz using the ZEL-SIP04-V02 impedance spectrometer (Forschungszentrum Julich

GmbH) [*Zimmermann et al*., 2007]. As in the case of the St Bees core samples, the sample holder described in *Binley et al*. [2005] was used for electrical measurements.

5.4. Dataset #4

Database #4 (Table 5) corresponds to the data reported in *Tong et al.* [2006a] (Table 1) who compiled a sizeable database of 123 samples from a shaly sand formation of the Daqing oilfield in China. The induced polarization measurements were performed in the time domain with a 120 s excitation time. This long time is probably required to polarize all the relevant polarization lengths scales existing in these sandstones (from clay minerals to the quartz grains). The observed voltage decay curves were inverted for the relaxation time distribution, the geometric mean of which is then referred to as the characteristic relaxation time (τ_{mD}). The gas permeability (corrected for the Klinkenberg effect) ranges between 0.1 mD to 770 mD and the porosity ranges between 0.071 and 0.215. The porosities for this database were determined using a helium porosimeter, while the permeabilities were determined using steady-state gas-flow tests [*Tong et al*., 2006a]. The samples were saturated by a 5 g L^{-1} NaCl solution. Since the molar mass of NaCl is 58.44276 g Mol^{-1}, this is equivalent to 0.086 M L^{-1}.

6. Interpretation of the Results

The modeled versus measured permeabilities are shown in Figures 13 to 17 for datasets #1 to #4. Figure 13 shows the predicted versus measured permeability (in mD) for the clean sands and high porosity Fontainebleau sandstones (dataset #1). We see that the model works very well and is typically able to predict the measured permeabilities inside half an order of magnitude. In the model we used the value for the diffusion coefficient $D_{(+)}$ (Na^+, 25°C) = 1.3×10^{-9} m^2 s^{-1}, consistent with clean silica. As discussed in Section 2, the model is expected to work well for such materials if the polarization length scale is also the length scale controlling flow properties through the pore network, that is, a characteristic pore size.

Figure 14 shows the predicted versus measured permeability for the datasets #2 and #3 taken together. These datasets include the Fontainebleau sandstones with porosity below 0.16 and various clayey sandstones. The model performs fairly well, generally inside one order of magnitude. We notice, however, that the model performance is weaker than that shown in Figure 13. There are also clearly some core samples for which the model overestimates the permeability by several orders of magnitude (3 orders of magnitude in the case of the Portland sandstone using the data from *Titov et al.* [2010]). These samples are characterized by high clay contents. We will come back to this point in the discussion.

Figure 15 shows a comparison between the prediction of the model and the experimental data for the St Bees sandstone (7 samples) and the Portland core sample we have measured (1 sample). The model predicts accurately the permeability of these two formations over four orders of magnitude.

Figure 16 shows the predicted versus measured permeability for the data from *Tong et al.* [2006a]. We use $D_{(+)}(\mathrm{Na}^+, 25°\mathrm{C}) = 3.8 \times 10^{-12}\ \mathrm{m}^2\mathrm{s}^{-1}$ assuming that we are dealing with clayey sandstones (but this is unclear from the paper of *Tong et al.* [2006a]) and we have multiplied all the time constants given by *Tong et al.* [2006a] by a constant factor (17.1). The relaxation times defined by the authors seem therefore proportional to the definitions we used earlier in Section 2. We have already discussed in Section 3 that several definitions exist for the relaxation times and great care should be exercised in using them. In other words, the measured permeability values from *Tong et al.* [2006a] are proportional to the ratio between the relaxation times to the formation factor, but the coefficient of proportionality has been empirically determined. The prediction of our formula works better than an order of magnitude for this database. In Figure 17, we combine the different databases (#1 to #4) and we see that our formula is able to predict the permeability inside plus or minus an order of magnitude.

7. Discussion

We first come back to the discrete values taken by the diffusion coefficients in our model. As outlined in Section 2.3, the mobility of the counterions in the Stern layer is related to the diffusion coefficient of the counterions by the Nernst-Einstein relationship $D_{(+)}^{S} = k_b T \beta_{(+)}^{S} / \left| q_{(+)} \right|$. In Figure 18, we plot the value of the measured permeability versus the ratio τ_0 / F. The data exhibit two distinct trends with diffusion coefficients consistent with the value of the mobility determined from the quadrature conductivity data shown in Figure 19 (data for this plot are provided in Tables 6 and 7). Once corrected for the effect of tortuosity and the effect of salinity, the data show two distinct trends evidencing two distinct values of the mobility of the counterions in the Stern layer. This implies in turn two distinct values of the diffusion coefficient for the counterions in the Stern layer. This consistency seems to validate the Stern layer model. In natural settings, it seems that only the clayey trend matters since the surface of silica will be usually contaminated with alumina and/or iron. Exceptions can, however, be expected as in the data reported by *Slater et al.* [2014].

The second point that deserves discussion is the choice of the characteristic relaxation time. As already discussed in Section 3, there are a number of ways of computing relaxation times that have been introduced in the literature. The relaxation times introduced in Figure 1 for two quite distinct types of spectra are probably the simplest one to estimate and to use to compute the permeability. Other types of characteristic times have been defined based on decomposition of the spectra using a specific function such as the Debye or Warburg functions. These decompositions lead to a (normalized) probability density of relaxation times from which some averaged or characteristic values can be determined such as the peak, the median, the arithmetic mean, or the geometric mean. We can therefore question the appropriateness of these characteristic times regarding the determination of the permeability. More work is needed here to investigate this issue.

The third point deserving some discussion concerns the limitation of the present approach. Some spectra do not show any characteristic relaxation time. In this case, it is better to use a relationship between the permeability, the intrinsic formation factor, and the quadrature conductivity as discussed by *Revil and Florsch* [2010] and very recently by *Weller et al.* [2015b]. Also Figures 14 and 16 shows that our model seems limited to permeability higher than 1 mD. For very low permeabilities, the intrinsic formation factor needs to be carefully investigated since the use of an apparent formation factor can overestimate the predicted permeability by more than order of magnitude and the use of a measurement at a single high salinity may fail to provide the intrinsic formation factor (see Figure 9b). The reason is that the high salinity range that can be used is limited by the saturation in salt of the brine while high surface conductivity can exist in smectite-rich rocks. This emphasizes the o use either multiple salinity datasets [*Vinegar and Waxman*, 1984] or the relationship between quadrature conductivity and surface conductivity, to remove the effect of surface conductivity as discussed by *Weller et al.* [2013].

The final point concerns the effect of the counterion. Usually in most ground waters, sodium is the main counterion. Exceptions exist for ground water in contact with carbonates for which Ca^{2+} can be the dominant cation. The effect of the cation on the polarization of the porous material was extensively discussed in *Vaudelet et al.* [2011a, b].

8. Conclusions

We have tested a simple equation to predict the permeability from the intrinsic formation factor and the characteristic relaxation time observed in the low-frequency quadrature conductivity of porous rocks. The prediction of this equation is very close to the measured permeability with an uncertainty typically within half an order of magnitude of permeability for permeabilities higher than 1 mD. For porous media that do not contain a significant amount of semi-conductors (e.g., pyrite, magnetite), this equation can be used to

provide an estimate of the permeability, usually inside one order of magnitude of the true values, also for clayey materials with dispersed clays. This approach is, however, valid only if a characteristic relaxation time can be defined in the spectra. When this is not the case, *Revil and Florsch* [2010] and *Weller et al*. [2015b] have shown that we can still get an approximate estimate of the permeability from the intrinsic formation factor and the quadrature conductivity instead of the relaxation time.

Our approach also relies on two values of the diffusion coefficient used to convert the main relaxation time into a pore size. The choice of the value of the diffusion coefficient is based on the properties of the mineral surface: pure silica and clays exhibit very different behaviors. That said, a small amount of alumina can strongly modify the properties of the silica as discussed by *Iler* [1979]. The internal consistency of the Stern layer model used in this work is supported by the fact that the two values of the diffusion coefficients are consistent with the two values of the mobility of the counterions in the Stern layer used to assess the low- and high-asymptotic conductivities.

Acknowledgments. We thank the Office of Science (BER), US. Department of Energy (award DE-FG02-08ER646559). A. Revil thanks T.K. Young for his work as department head of the department of Geophysics of the Colorado School of Mines. We thank Nikita Seleznev (Schlumberger) for the Portland sample. A. Binley is grateful to D. Lesmes, S. Kruschwitz and A. Butcher for providing samples used in Dataset #3. All the data reported in this paper can be obtained from A. Binley (a.binley@lancaster.ac.uk) and A. Revil (arevil@mines.edu) and will be available as text files in ResearchGate. We thank Andreas Kemna for useful discussions. We thank the Associate Editor S. Huisman and the three referees, A. Weller, M. Ingham, and K. Titov for careful and very constructive comments that have strongly improved the manuscript.

Appendix A. The Cole Cole Model

A very popular complex conductivity model is the Cole-Cole function:

$$\sigma^*(\omega) = \sigma_\infty - \frac{M_n}{1+\left(i\omega\tau_0\right)^c}, \tag{A1}$$

[*Cole and Cole*, 1941] and where the normalized chargeability is traditionally defined by $M_n = \sigma_\infty - \sigma_0 \geq 0$, the chargeability is $M = 1 - \sigma_0 / \sigma_\infty$, and c denotes the Cole-Cole exponent. In Eq. (4), τ_0 denotes the characteristic relaxation time (or time constant), and σ_0 and σ_∞ denote the low-frequency and high-frequency asymptotic limits of the electrical conductivity. The in phase and quadrature components of the complex conductivity are,

$$\sigma' = \sigma_\infty - \frac{1}{2} M_n \left\{ 1 - \frac{\sinh\left[c \ln\left(\omega\tau_0\right)\right]}{\cosh\left[c \ln\left(\omega\tau_0\right)\right] + \sin\left[\frac{\pi}{2}(1-c)\right]} \right\}, \tag{A2}$$

$$\sigma'' = -\frac{1}{2} \frac{M_n \cos\left[\frac{\pi}{2}(1-c)\right]}{\cosh\left[c \ln\left(\omega\tau_0\right)\right] + \sin\left[\frac{\pi}{2}(1-c)\right]}, \tag{A3}$$

respectively. At the critical frequency $\omega_c = 1/\tau_0$, the quadrature conductivity is related to the normalized chargeability by,

$$\sigma''(\omega = \omega_c) = -\frac{1}{2} \frac{\cos\left[\frac{\pi}{2}(1-c)\right]}{1 + \sin\left[\frac{\pi}{2}(1-c)\right]} M_n. \tag{A4}$$

As discussed in *Revil et al.* [2014a], we have $0 \leq c \leq 0.6$, i.e., even for a very narrow pore size or grain size distribution, the Cole-Cole exponent c is never much above the value c = ½, corresponding to a Warburg function. The physical reasons for this behavior are explored in *Revil et al.* [2014a]. Cole-Cole spectra for c close to zero correspond to very flat spectra in the frequency domain and are not of high interest here. For $c = 1/2$, we have,

$$\sigma''(\omega = \omega_c) = -\frac{1}{2}\left(\frac{\sqrt{2}}{2+\sqrt{2}}\right) M_n \approx -\frac{1}{5} M_n. \tag{A5}$$

Eq. (A5) means that the quadrature conductivity taken at (or close to) the relaxation peak is proportional to the normalized chargeability, which can be determined either from frequency

domain induced polarization data (using the behavior of the real part of the conductivity versus the frequency) or from time domain induced polarization data [*Fianduca et al.*, 2012]. In this second case, it is important that the duration of the primary current be long enough to polarize all the pores of the porous material. For instance *Tong et al*. [2006a, b] use a polarization time of 120 s. In the frequency dependent conductivity model obtained through a volume-averaging approach by *Revil* [2013a, b], the low- and high frequency conductivities entering Equations (1) and (2) are given by:

$$\sigma_0 = \frac{1}{F}\sigma_w + \left(\frac{1}{F\phi}\right)\rho_S \beta_{(+)}(1-f)\mathrm{CEC}, \tag{A6}$$

$$\sigma_\infty = \frac{1}{F}\sigma_w + \left(\frac{1}{F\phi}\right)\rho_S \left[\beta_{(+)}(1-f) + \beta_{(+)}^S f\right]\mathrm{CEC}, \tag{A7}$$

where ϕ (dimensionless) denotes the connected porosity, F (dimensionless) denotes the (intrinsic) electrical formation factor related to the connected porosity by Archie's law $F = \phi^{-m}$ where $m \geq 1$ is known as the first Archie's exponent, cementation exponent or porosity exponent [*Archie*, 1942], σ_w (in S m^{-1}) corresponds to the pore water conductivity, and f (dimensionless) denotes the fraction of counterions in the Stern layer (typically ~0.90 for clays, see *Revil* [2013a, b]). In Equations (7) and (8), ρ_S denotes the mass density of the solid phase (typically 2650 kg m^{-3} for silica minerals and 2700 kg m^{-3} for clay minerals), $\beta_{(+)}$ and $\beta_{(+)}^S$ have been defined in the main text and the CEC denotes the cation exchange capacity of the material (expressed in C kg^{-1}). The cation exchange capacity corresponds to the total amount of cations that can get sorbed on the surface of a mineral. For silica grains, *Revil* [2013b] proposed the following relationship: CEC = 6 Q_S / (ρ_s d) with Q_S = 0.64 C m^{-2} and ρ_s = 2650 kg m^{-3} and where d denotes the mean grain diameter.

References

Aal, G, and A. Estella (2013), Spectral induced polarization (SIP) response of biodegraded oil in porous media, Geophysical Journal International, doi: 10.1093/gji/ggt416.

Aal, G., E.A. Atekwana, and A. Revil (2014), Geophysical signatures of disseminated iron minerals: A proxy for understanding subsurface biophysicochemical processes, *Journal of Geophysical Research-Biogeosciences*, *119*(9), 1831-1849, doi: 10.1002/2014JG002659, 2014

Allen, D.J., L.J., Brewerton, L.M., Coleby, B.R., Gibbs, M.A., Lewis, A.M., MacDonald, S.J. Wagstaff, and A.T. Williams (1997), The physical properties of major aquifers in England and Wales. British Geological Survey Technical Report WD/97/34. *Environment Agency R&D Publication, 8*.

Avellaneda, M., and S. Torquato (1991) Rigorous link between fluid permeability, electrical conductivity, and relaxation times for transport in porous media, *Physics of Fluids A*, *3*, 2529–2540.

Bernabé, Y., and A. Revil, (1995), Pore-scale heterogeneity, energy dissipation and the transport properties of rocks, *Geophysical Research Letters*, *22*(12), 1529-1552.

Binley, A., L.D., Slater, M., Fukes, and G. Cassiani (2005), Relationship between spectral induced polarization and hydraulic properties of saturated and unsaturated sandstone, *Water Resources Research*, *41*, W12417, doi:10.1029/2005WR004202.

Bolève, A., A. Crespy, A. Revil, F. Janod, and J. L. Mattiuzzo (2007), Streaming potentials of granular media: Influence of the Dukhin and Reynolds numbers, *Journal of Geophysical Research*, *112*, B08204, doi:10.1029/2006JB004673.

Bouchedda, A., M., Chouteau, A., Binley, and B. Giroux (2012), 2-D Joint structural inversion of cross-hole electrical resistance and ground penetrating radar data, *Journal of Applied Geophysics*, *78*, 52-57.

Börner, F. D. (1992), Complex conductivity measurements of reservoir properties, Proceedings of the Third European Core Analysis Symposium, 359-386.

Börner, F. D., J. R. Schopper, and A. Weller (1996), Evaluation of transport and storage properties in the soil and groundwater zone from induced polarization measurements, *Geophysical Prospecting*, *44*, 583-601.

Breede, K., A. Kemna, O. Esser, E. Zimmermann, H. Vereecken, and J.A. Huisman (2012), Spectral induced polarization measurements on variably saturated sand-clay mixtures, *Near Surface Geophysics*, *10*, doi:10.3997/1873-0604.2012048.

Carroll, S., R. S., Maxwell, W., Bourcer, S., Martin, and S. Hulsey (2002), Evaluation of silica-water surface chemistry using NMR spectroscopy, *Geochimica et Cosmochimica Acta*, *66*(6), 913–926, doi: 10.1016/S0016-7037(01)00827-4.

Chappex, T. and K.L. Scrivener (2012), The influence of aluminium on the dissolution of amorphous silica and its relation to alkali silica reaction, *Cement and Concrete Research*, *42*, 1645–1649.

Cole, K.S. and R.H. Cole (1941), Dispersion and absorption in dielectrics. I. Alternating current characteristics, *J. Chem. Phys.*, *9***,** 341–351.

Doetsch, J., N., Linde and A. Binley, (2010), Structural joint inversion of time-lapse crosshole ERT and GPR traveltime data, *Geophys. Res. Lett.*, *37*, L24404, doi: 10.1029/2010GL045482.

Fianduca G., E. Auken, A. Vest Christiansen, and A. Gazoty (2012), Time-domain-induced polarization: Full-decay forward modeling and 1D laterally constrained inversion of Cole-Cole parameters, Geophysics, *77*(3), E213–E225, doi: 10.1190/GEO2011-0217.1.

Florsch, N., C. Camerlynck, and A. Revil (2012), Direct estimation of the distribution of relaxation times from induced-polarization spectra using a Fourier transform analysis, *Near Surface Geophysics*, *10***,** 517–531.

Florsch, N., M., Llubes, F., Téreygeol, A. Ghorbani, and P. Roblet (2011), Quantification of slag heap volumes and masses through the use of induced polarization: Application to the Castel-Minier site, *Journal of Archaeological Science*, *38*, 438–451.

Florsch, N., A., Revil, and C. Camerlynck (2014), Inversion of generalized relaxation time distributions with optimized damping parameter, *Journal of Applied Geophysics*, *109*, 119–132.

Fuller, B.D., and S. H. Ward (1970), Linear system description of the electrical parameters of rocks, *IEEE Trans. Geosci. Electron.*, *8*, 7–18.

Grosse, C. (2009), Generalization of a classic thin double layer polarization theory of colloidal suspensions to electrolyte solutions with different ion valences, *Journal Physical Chemistry B*, *113*, 8911–8924.

Grunat D.A., L.D. Slater, and M. Wehrer (2013), Complex electrical measurements on an undisturbed soil core: evidence for improved estimation of saturation degree from imaginary conductivity, *Vadose Zone Journal*, 1-13, doi:10.2136/vzj2013.03.0059.

Ishido, T., and H. Mizutani (1981), Experimental and theoretical basis of electrokinetic phenomena in rock-water systems and its applications to geophysics, *Journal of Geophysical Research*, *86*(B3), 1763–1775.

Johnson, D. L., T. J. Plona, and H. Kojima (1986), Probing porous media with 1st sound, 2nd sound, 4th sound and 3rd sound, in *Physics and Chemistry of Porous Media*, vol. 2, edited by R. Jayanth, J. Banavar, and K. W. Winkler, pp. 243–277, Am. Inst. Phys., New York.

Joseph, S., Ingham, M. and Gouws, G. (2015), Spectral induced polarization measurements on New Zealand sands - dependence on fluid conductivity, *Near Surface Geophysics*, *12*, doi: 10.3997/1873-0604.2014043.

Karaoulis, M., A., Revil, D.D., Werkema, B., Minsley, W.F. Woodruff, and A. Kemna (2011), Time-lapse 3D inversion of complex conductivity data using an active time

constrained (ATC) approach, *Geophysical Journal International*, *187*, 237–251, doi: 10.1111/j.1365-246X.2011.05156.x.

Keery, J., A., Binley, A., Elshenawy, and J. Clifford (2012), Markov-chain Monte Carlo estimation of distributed Debye relaxations in spectral induced polarization, *Geophysics*, *77*(2), E159–E170, doi: 10.1190/GEO2011-0244.1.

Keller, G.V. (1988), Rock and mineral properties, in: M.N. Nabighian (Ed.), Electromagnetic Methods in Applied Geophysics, in: *Soc. of Expl. Geophys.*, *1*, 13–51.

Kemna, A., A., Binley and L. Slater (2004), Crosshole IP imaging for engineering and environmental applications, *Geophysics*, *69*(1), 97-107.

Kemna, A., Huisman, J.A., Zimmermann, E., Martin, R., Zhao, Y., Treichel, A., Flores Orozco, A., and Fechner, T. (2014), Broad-band electrical impedance tomography for subsurface characterization using improved corrections of electromagnetic coupling and spectral regularization, in Weber, M. and Münch, U., Eds., Tomography of the Earth's Crust: From Geophysical Sounding to Real-Time Monitoring, Geotechnologien Science Report No. 21, doi:10.1007/978-3-319-04205-3, 1-20.

Klinkenberg, L. J. (1941), The permeability of porous media to liquids and gases, *Drilling and Production Practice*, *American Petroleum Inst*., 200–213

Koch, K., A., Kemna, J., Irving, and K. Holliger (2011), Impact of changes in grain size and pore space on the hydraulic conductivity and spectral induced polarization response of sand, *Hydrology and Earth System Science*, *15*, 1785-1794.

Koch, K., A. Revil, and K. Holliger (2012), Relating the permeability of quartz sands to their grain size and spectral induced polarization characteristics, *Geophysical Journal International*, *190*, 230-242.

Kruschwitz, S., A., Binley, D., Lesmes, and A. Elshenawy (2010), Textural controls on low frequency electrical spectra of porous media, *Geophysics*, *75*(4), WA113-WA123.

Lesmes, D. P. and K.M. Frye (2001), Influence of pore fluid chemistry on the complex conductivity and induced polarization responses of Berea sandstone, *J. geophys. Res.*, *106*(B3), 4079–4090.

Lesmes, D.P. and F.D. Morgan (2001), Dielectric spectroscopy of sedimentary rocks, *J. geophys. Res.*, *106*(B7), 13 329–13 346.

Linde, N., A., Binley, A., Tryggvason, L. B. Pedersen, and A. Revil (2006), Improved hydrogeophysical characterization using joint inversion of cross-hole electrical resistance and ground-penetrating radar traveltime data, *Water Resour. Res.*, *42*, W12404, doi:10.1029/2006WR005131.

Lorne, B., F. Perrier, and J.-P. Avouac, (1999), Streaming potential measurements. 1. Properties of the electrical double layer from crushed rock samples, *Journal of Geophysical Research*, *104***,** 17 857–17 877.

MacLennan, K., M. Karaoulis, and A. Revil (2014), Complex conductivity tomography using low-frequency cross-well electromagnetic data, *Geophysics*, *79*(1), E23-E38, doi: 10.1190/GEO2012-0531.1.

Mortland, M. M., and J. L. Mellor, 1954, Conductometric titration of soils for cation exchange capacity, *Proc. Soil. Sci. Soc. Am.*, *18*, 363-364.

Nordsiek, S. and A. Weller (2008), A new approach to fitting induced-polarization spectra, *Geophysics*, *73*(6), F235 – F245.

Okay, G., P. Leroy, A. Ghorbani, P. Cosenza, C. Camerlynck, J. Cabrera, N. Florsch, and A. Revil, 2014, Spectral induced polarization of clay-sand mixtures. Experiments and modeling, *Geophysics*, *79*(6), E353-E375, doi: 10.1190/GEO2013-0347.1.

Pape, H., and D. Vogelsang (1996), Fractal evaluation of induced polarization logs in the KTB-Obrpfalz HB, *Bundesanstalt fur Geowissenschaften und Rohstoffe / Geologische Landesämter in der Bundesrepublik Deutschland, Geologisches Jahrbuch*, *54*(E), 3-27.

Revil, A., L.M., Cathles, S., Losh, and J.A. Nunn (1998), Electrical conductivity in shaly sands with geophysical applications, *Journal of Geophysical Research*, *103*(B10), 23,925-23,936.

Revil, A. and N. Florsch (2010) Determination of permeability from spectral induced polarization in granular media, *Geophys. J. Int.*, *181*(3), 1480-1498.

Revil, A. and M. Skold (2011). Salinity dependence of spectral induced polarization in sands and sandstones, *Geophys. J. Int.*, *187*, 813–824, doi: 10.1111/j.1365-246X.2011.05181.x.

Revil, A. (2012), Spectral induced polarization of shaly sands: Influence of the electrical double layer, *Water Resources Research*, *48*, W02517, doi:10.1029/2011WR011260.

Revil, A., K., Koch, and K. Holliger (2012), Is it the grain size or the characteristic pore size that controls the induced polarization relaxation time of clean sands and sandstones? *Water Resour. Res.*, *48*, W05602, doi:10.1029/2011WR011561.

Revil, A. (2013a), On charge accumulations in heterogeneous porous materials under the influence of an electrical field, *Geophysics*, *78*(4), D271–D291, doi: 10.1190/GEO2012-0503.1.

Revil, A. (2013b) Effective conductivity and permittivity of unsaturated porous materials in the frequency range 1 mHz–1GHz, *Water Resour. Res.*, *49*, doi: 10.1029/2012WR012700.

Revil, A., M., Skold, S., Hubbard, Y., Wu, D., Watson, and M. Karaoulis (2013a), Petrophysical properties of saprolites from the Oak Ridge Integrated Field Research Challenge site, Tennessee, *Geophysics*, *78*(1), D21–D40, doi: 10.1190/geo2012-0176.1.

Revil A., W.F. Woodruff, C. Torres-Verdín, and M. Prasad (2013b), Complex conductivity tensor of hydrocarbon-bearing shales and mudrocks, *Geophysics*, *78*(6), D403-D418, doi: 10.1190/GEO2013-0100.1.

Revil, A., Y. Wu, M. Karaoulis, S. S. Hubbard, D. B. Watson, and J. D. Eppehimer (2013c), Geochemical and geophysical responses during the infiltration of fresh water into the contaminated saprolite of the Oak Ridge Integrated Field Research Challenge site, Tennessee, *Water Resour. Res.*, *49*, doi:10.1002/wrcr.20380.

Revil., A. (2014), Comment on: "On the relationship between induced polarization and surface conductivity: Implications for petrophysical interpretation of electrical measurements" (A. Weller, L. Slater, and S. Nordsiek, Geophysics, 78, no. 5, D315–D325), *Geophysics*, *79*(2), X1-X5, doi: 10.1190/GEO2013-0300.1.

Revil, A., N., Florsch, and C. Camerlynck (2014a), Spectral induced polarization porosimetry, *Geophys. J. Int.*, *198*, 1016–1033, doi: 10.1093/gji/ggu180.

Revil, A., P., Kessouri, and C. Torres-Verdín (2014b), Electrical conductivity, induced polarization, and permeability of the Fontainebleau sandstone, *Geophysics*, *79*(5), D301–D318, doi: 10.1190/GEO2014-0036.1.

Schmutz, M., A. Revil, P. Vaudelet, M. Batzle, P. Femenia Vinao, and D.D. Werkema (2010), Influence of oil saturation upon spectral induced polarization of oil bearing sands: *Geophysical Journal International*, *183***,** 211–224.

Schmutz, M., A. Blondel, and A. Revil (2012), Saturation dependence of the quadrature conductivity of oil-bearing sands, *Geophysical Research Letters*, *39*, L03402, doi:10.1029/2011GL050474.

Schwarz, G. (1962) A theory of the low-frequency dispersion of colloidal particles in electrolyte solution, *Journal of Physical Chemistry*, *66*, 2636–2642.

Schwartz, N., T. Shalem and A. Furman (2014), The effect of organic acid on the spectral-induced polarization response of soil, *Geophysical Journal International*, doi: 10.1093/gji/ggt529.

Scott, J. and R. Barker (2003), Determining pore-throat size in Permo-Triassic sandstones from low-frequency electrical spectroscopy, *Geophys. Res. Lett.*, *30*, 1450, doi:10.1029/2003GL016951.

Shefer, I., N. Schwartz, and A. Furman (2013), The effect of free-phase NAPL on the spectral induced polarization signature of variably saturated soil, *Water Resour. Res.*, *49*, doi:10.1002/wrcr.20502.

Slater, L. and D.P. Lesmes, (2002), Electrical-hydraulic relationships observed for unconsolidated sediments, *Water Resour. Res.*, *38*(10), 1213, doi: 10.1029/2001WR001075.

Slater, L., W. Barrash, J. Montrey, and A.Binley (2014), Electrical-hydraulic relationships observed for unconsolidated sediments in the presence of a cobble framework, *Water Resour. Res.*, *50*, doi:10.1002/2013WR014631.

Tarasov, A., and K. Titov (2013), On the use of the Cole–Cole equations in spectral induced polarization, *Geophysical Journal International*, *195*, 352-356.

Tarasov, A., K. Titov, M., Münch, and A., Kemna, (2003), Induced polarization spectra of sands and clays measured in the time domain: Proc. Int. Conf. Geophysics of the 21st Century – a Leap into the Future, Moscow, 6-10 September 2003, PS11, P6, 4 p.

Titov, K., V. Komarov, V. Tarasov, and A. Levitski, (2002), Theoretical and experimental study of time-domain induced polarization in water saturated sands, *J. Appl. Geophys.*, *50*, 417–433.

Titov, K., A., Tarasov, Y., Ilyn, N. Seleznev, and A., Boyd, (2010), Relationships between induced polarization relaxation time and hydraulic properties of sandstone, *Geophys. J. Int*., *180*, 1095-1106, doi: 10.1111/j.1365-246X.2009.04465.x.

Tong, M., L., Li, W., Wang, and Y. Jiang (2006a), A time-domain induced-polarization method for estimating permeability in a shaly sand reservoir, *Geophysical Prospecting*, *54*, 623–631.

Tong, M., L., Li, W., Wang, and Y. Jiang, (2006b), Determining capillary-pressure curve, pore-size distribution, and permeability from induced polarization of shaley sand, *Geophysics*, *71*, N33–N40.

Van Olphen, H., and M. H. Waxman (1958), Surface conductance of sodium bentonite in water, *Proceedings of the Fifth National Conference, Clays and Clay Minerals, NAS-RRC Pub.*, *566*, 61–80.

Vaudelet, P., A. Revil, M. Schmutz, M. Franceschi, and P. Bégassat (2011a), Induced polarization signature of the presence of copper in saturated sands, *Water Resources Research*, *47*, W02526, doi:10.1029/2010WR009310.

Vaudelet, P., A. Revil, M. Schmutz, M. Franceschi, and P. Bégassat, (2011b), Changes in induced polarization associated with the sorption of sodium, lead, and zinc on silica sands, *Journal of Colloid and Interface Science*, *360*, 739-752.

Vinegar, H.J. and M.H. Waxman (1984), Induced polarization of shaly sands, *Geophysics*, *49*, 1267–1287.

Vinegar, H.J. and M.H. Waxman (1988), In-situ method for determining formation permeability. *U.S. Patent*, *4* (743), 854.

Weigand, M., and A. Kemna (2015), Debye decomposition of time-lapse spectral induced polarisation data, submitted to *Computers & Geosciences.*

Weller, A., K., Breede, L. Slater, and S. Nordsiek (2011), Effect of changing water salinity on complex conductivity spectra of sandstones, *Geophysics*, *76*(5), F315-F327, doi: 10.1190/GEO2011-0072.1.

Weller, A., L., Slater, and S. Nordsiek (2013), On the relationship between induced polarization and surface conductivity: Implications for petrophysical interpretation of electrical measurements, *Geophysics*, *78*(5), D315–D325, doi: 10.1190/geo2013-0076.1.

Weller, A., L. Slater, J. A. Huisman, O. Esser, F. H. Haegel (2015a). On the specific polarizability of sands and sand-clay mixtures, *Geophysics*, *80*(3), A57-A61. doi: 10.1190/geo2014-0509.1.

Weller, A., L. Slater, A. Binley, S. Nordsiek, and S. Xu (2015b), Permeability prediction based on induced polarization: Insights from measurements on sandstone and unconsolidated samples spanning a wide permeability range, *Geophysics 80*(2), D161-D173.

Wong, J. (1979), An electrochemical model of the induced polarization phenomenon in disseminated sulfide ores, *Geophysics*, *44*, 1245–1265, doi: 10.1190/1.1441005.

Woodruff W. F., A. Revil, and C. Torres-Verdín (2014), Laboratory determination of the complex conductivity tensor of unconventional anisotropic shales, *Geophysics, 79*(5), E183–E200, doi: 10.1190/GEO2013-0367.1,

Worthington, P.F. and F.A. Collar (1984), Relevance of induced polarization to quantitative formation evaluation, *Marine and Petroleum Geology*, *1*, 14–26.

Zhou, J., A., Revil, M., Karaoulis, D., Hale, J., Doetsch, and S. Cuttler (2014), Image-guided inversion of electrical resistivity data, *Geophys. J. Int.*, *197*, 292-309, doi:10.1093/gji/ggu001.

Zimmermann, E., J., Berwix, W., Glaas, H., Meier, H.M. Münch, and A. Kemna, (2007). ZEL-SIP04-V02: User manual. Forschungszentrum Julich GmbH.

Zisser, N., A., Kemna, and G. Nover (2010), Relationship between low-frequency electrical properties and hydraulic permeability of low-permeability sandstones, *Geophysics*, *75*(3), E131-E141, doi: 10.1190/1.3413260.

Table 1. Dataset #1. Petrophysical properties for the clean sands (16 samples from *Koch et al.* [2011]), the high-porosity Fontainebleau sandstones (3 samples, this work), and three other samples (sands and sandstones) from various papers. The characteristic relaxation time τ_0 is obtained from the peak frequency f_p (see main text). This database comprises a total of 23 samples. All the measurements have been done in the frequency domain. "Type" refers to the type of spectrum: peak frequency (P) or corner (C) frequency.

Sample	k (mD)	F (-)	ϕ (-)	τ_0 (s)	Type
F36 (1)	17,600	3.77	0.44	0.44	P
F32 (1)	53,100	3.55	0.44	0.51	P
WQ1 (1)	129,000	3.25	0.47	2.13	P
SP1 (1)	20,800	3.14	0.46	0.30	P
SP2 (1)	33,000	3.40	0.44	0.30	P
SP4 (1)	171,000	3.12	0.49	0.84	P
SP5 (1)	280,000	3.10	0.48	4.68	P
SP6 (1)	394,000	3.34	0.49	12.4	P
F36-C (1)	11,100	4.12	0.38	0.23	P
F32-C (1)	24,000	3.75	0.39	0.14	P
WQ1-C (1)	75,000	3.97	0.42	1.86	P
SP1-C (1)	11,700	3.23	0.41	0.14	P
SP2-C (1)	19,800	3.55	0.39	0.40	P
SP4-C (1)	105,000	3.52	0.44	0.80	P
SP5-C (1)	196,000	3.36	0.43	3.65	P
SP6-C (1)	256,000	3.63	0.43	3.42	P
M11 (2)	1,430	17.2	0.16	0.08	C
Z17Z (2)	3,390	12.7	0.19	0.16	P
Z04Z1 (2)	3,560	10.1	0.22	0.16	P
S2 (3)	23,000	2.47	0.47	1.10	P
U30 (4)	247,000	3.60	0.41	70	P
Bu12 (5)	114	18.0	0.18	0.0032	P

(1) From *Koch et al.* [2011, 2012]. Clean silica sands.
(2) This work. High-porosity Fontainebleau sandstones (porosity above 0.16).
(3) From *Joseph et al.* [2015] New-Zealand sand.
(4) From *Revil and Skold* [2011]. Pure silica sand.
(5) From *Weller et al.* [2011]. Sandstone. Quartz (~90%), plagioclase and mica (~5%).

Table 2. Dataset #2. Petrophysical properties for the clayey sandstones (6 samples from *Revil et al*. [2014a]), the low-porosity Fontainebleau sandstones (12 samples), one saprolite sample (S16), one Berea sandstone, one Cretaceous sandstone from the "Münsteraner Bucht" in northern Germany (GR), and a fine-grained silty sandstone (Bu3). We have also added 6 additional sandstones from the study of *Titov et al*. [2010] (including one Portland sandstone core), 7 new samples from the St Bees sandstones (see Figure 4), and one new sample of the Portland formation (see Figure 6). This database includes a total of 35 samples all performed in the frequency domain except for the work of *Titov et al*. [2010]. For the Portland sample investigated by *Titov et al*. [2010] the reported formation factor (3.29) was incompatible with a cementation exponent *m* larger than 1 indicating clearly that the formation factor was an apparent formation factor. "Type" refers to the type of spectrum: peak frequency (P) or corner (C) frequency.

Sample	k (mD)	F (-)	ϕ (-)	τ_0 (s)	Type
S499 (1)	1103	5.6	0.265	2.6	P
S498 (1)	35.9	9.0	0.206	0.20	P
S490 (1)	635	12.1	0.233	3.2	P
S493 (1)	115	18.3	0.232	0.41	P
S439 (1)	2.62	13.3	0.208	0.023	P
S436 (1)	1623	4.0	0.306	25.5	P
Z02Z (2)	2.49	84.6	0.050	0.16	C
M12 (2)	2.17	289	0.051	0.53	C
Z18X (2)	1.20	183	0.052	0.27	C
Z20Y (2)	4.7	141	0.052	0.20	C
Z01Z (2)	6.3	99.6	0.057	0.080	C
M14 (2)	44.4	92.1	0.077	7.96	C
Z05Y (2)	42.3	51.4	0.084	5.31	C
Z15X (2)	182	27.7	0.092	5.31	C
Z13X1 (2)	190	40.8	0.100	7.96	C
Z03Y (2)	154	38.2	0.106	8.84	C
Z16X (2)	15.7	38.9	0.069	0.20	P
Z18Y (2)	1.30	180.9	0.047	4.0	C
S16 (3)	5.0	5.9	0.49	0.013	P
Berea (4)	102	18.5	0.18	7.96	C
GR (5)	330	9.8	0.25	3.98	P
Bu3 (5)	0.02	68.5	0.09	1.59	P
Portland (6)	0.42	15.8	0.197	1.4	-
Boise264 (6)	604	13.7	0.256	3.2	-
Bandera274 (6)	19.4	11.9	0.208	2.0	-
Massilon1065 (6)	1091	12.9	0.220	20	-
Berea100 (6)	258	18.8	0.202	2.2	-
Berea400 (6)	843	14.0	0.236	2.0	-
SB1 (7)	366	11.0	0.27	0.989	P
SB2 (7)	4.9	22.4	0.20	0.147	P
SB3 (7)	2.3	29.0	0.21	0.061	P

SB4 (7)	14.5	21.7	0.25	0.137	P
SB5 (7)	0.55	43.3	0.20	0.013	P
SB6 (7)	0.04	49.3	0.18	0.004	P
SB7 (7)	0.71	57.1	0.14	0.067	P
PS1 (8)	0.10	43.8	0.194	0.0021	P

(1) From *Revil et al*. [2014a]. Clayey sandstones.
(2) This work. Low-porosity Fontainebleau sandstones (porosity below 0.11).
(3) From *Revil et al.* [2013]. Saprolite
(4) From *Lesmes and Fry* [2001] and *Lesmes and Morgan* [2001]. Berea sandstone (KCl)
(5) From *Weller et al.* [2011].
(6) From *Titov et al.* [2010].
(7) This work. St Bees sandstone.
(8) This work. Portland sample.

Table 3. Composition (in weight fractions) of the core samples used by Titov *et al.* [2010]. I: Illite, S: Smectite, K: Kaolinite, F: Feldspar, C: Carbonate, and Q: Quartz. Note that the Portland sample is the sample characterized by the highest amount of clay minerals (courtesy: Konstantin Titov and Nikita Seleznev).

Sample	I	S	K	Clay	F	C	Q
Berea 100	3.4	0.0	2.6	6.1	4.4	3.9	84.4
Berea 400	2.5	0.0	2.7	5.2	3.9	1.1	88.6
Boise 264	2.0	4.5	0.0	6.4	45.2	0.8	44.6
Massilon 1065	2.4	0.0	1.3	3.7	0.0	3.9	88.0
Portland	6.9	0.0	24.2	31.2	9.1	22.6	28.4
Bandera 274	12.5	0.0	3.8	20.2	13.7	1.1	58.6

Table 4. Dataset #3. This dataset comprises a total of 18 samples and is new (frequency-domain measurements). The formation factor is determined at high salinity of 1 M L^{-1} NaCl and is considered to be an intrinsic formation factor. "Type" refers to the type of spectrum: peak frequency (P) or corner (C) frequency. The three Sherwood samples were previously considered in Binley et al. [2005] but spectra have been re-measured for this work using a NaCl saturating fluid. For samples PB5, AC2, and 5T, the value is reported at the measurement limit. For this dataset, we apply the value of the diffusion coefficient for clayey sandstones ($D_{(+)}$ (Na^+, 25°C) = 3.8×10^{-12} m^2s^{-1}).

Sandstone	Sample	k (mD)	F (-)	ϕ (-)	τ_0 (s)	Type
Bentheimer	Be1	250.00	22.42	0.19	0.848	P
Obernkirchener	O5	50.50	17.50	0.18	0.855	P
Gravenhorster	G4	5.73	27.55	0.14	0.927	P
Coconino	Co7	2.63	48.10	0.11	0.553	P
Cottaer	C33	2.60	15.32	0.22	1.218	P
Berea	4B11	215.00	15.19	0.19	1.668	P
Clashach	CLASH	523.00	14.39	0.17	3.193	P
Elb	E3	4640.00	15.23	0.19	1.800	P
Penn. Blue	PB5	<1.00	141.98	0.04	1.343	P
Arizona Chocolate	AC2	<0.01	120.74	0.09	0.123	P
Arizona Chocolate	AC4	0.05	115.71	0.09	0.191	P
Tennessee	2T	0.02	151.38	0.05	6.326	P
Tennessee	5T	<0.01	143.34	0.06	5.668	P
Island Rust	IR01	13.25	37.80	0.14	1.322	P
Island Rust	IR02	22.32	33.90	0.15	1.403	P
Sherwood	VEG2RI-2	4300.49	8.60	0.31	2.043	P
Sherwood	VEC15-5	73.41	8.21	0.31	0.343	P
Sherwood	HEC18-7	52.73	9.31	0.26	0.404	P

Table 5. Dataset #4 from *Tong et al*. [2006a] (clayey sandstones). The formation factor is here determined from the porosity using $F = \phi^{-2}$ (classical Archie's law). This database includes a total of 123 samples. The quantity τ_g denotes the relaxation time reported by *Tong et al*. [2006a] (corresponding to τ_{mD} in the main text).

Sample	k (mD)	F (-)	ϕ (-)	τ_g (ms)
1	770.00	22.041	0.213	370.80
2	663.00	24.507	0.202	643.90
3	519.00	27.127	0.192	679.10
4	450.00	26.031	0.196	476.50
5	447.00	23.338	0.207	374.10
6	402.00	27.701	0.190	716.30
7	400.00	24.507	0.202	616.20
8	370.00	28.293	0.188	496.90
9	370.00	34.199	0.171	756.60
10	351.00	29.861	0.183	360.30
11	347.00	30.524	0.181	286.90
12	341.00	27.995	0.189	685.80
13	302.00	31.562	0.178	684.70
14	297.00	21.633	0.215	682.90
15	281.00	30.190	0.182	325.40
16	276.00	41.091	0.156	317.70
17	245.00	43.283	0.152	321.90
18	243.00	32.653	0.175	563.20
19	229.00	30.864	0.180	486.60
20	215.00	48.902	0.143	227.50
21	214.00	39.062	0.160	827.40
22	204.00	23.565	0.206	302.70
23	174.00	31.562	0.178	321.40
24	166.00	41.623	0.155	316.80
25	165.00	55.692	0.134	254.90
26	165.00	32.283	0.176	276.70
27	154.00	24.752	0.201	255.30
28	152.00	39.062	0.160	209.20
29	150.00	42.719	0.153	389.80
30	147.00	32.653	0.175	226.40
31	147.00	34.199	0.171	178.50
32	115.00	35.856	0.167	116.90
33	110.00	30.524	0.181	219.40
34	101.00	30.190	0.182	123.80
35	94.600	31.919	0.177	232.80
36	92.600	30.864	0.180	195.30
37	66.300	49.593	0.142	99.400
38	64.300	33.802	0.172	152.60
39	64.100	35.013	0.169	288.50
40	61.700	38.579	0.161	267.00
41	34.300	50.299	0.141	86.900
42	34.000	55.692	0.134	240.70
43	33.600	90.703	0.105	148.30
44	32.500	39.062	0.160	175.10
45	31.900	31.919	0.177	100.10
46	16.300	60.093	0.129	95.300
47	16.000	53.279	0.137	57.900
48	15.900	27.701	0.190	32.100
49	15.800	73.051	0.117	58.700
50	15.700	58.272	0.131	46.900
51	15.400	58.272	0.131	98.100
52	10.000	53.279	0.137	50.100
53	10.000	81.162	0.111	53.400

54	8.5000	36.731	0.165	32.400
55	8.4000	56.532	0.133	17.300
56	8.1000	68.301	0.121	111.20
57	8.0000	45.043	0.149	31.500
58	7.7000	73.051	0.117	47.900
59	7.2000	48.225	0.144	21.700
60	7.1000	45.654	0.148	32.100
61	7.0000	62.000	0.127	25.200
62	6.9000	43.858	0.151	39.600
63	6.6000	65.036	0.124	31.200
64	6.6000	108.51	0.0960	39.400
65	6.4000	198.37	0.0710	52.700
66	6.3000	141.72	0.0840	30.900
67	6.2000	46.913	0.146	36.500
68	6.1000	75.614	0.115	38.100
69	6.1000	43.283	0.152	28.800
70	6.0000	56.532	0.133	42.300
71	6.0000	37.638	0.163	77.600
72	6.0000	46.277	0.147	46.800
73	5.9000	192.90	0.0720	67.100
74	3.5000	126.25	0.0890	26.400
75	3.4000	129.13	0.0880	29.900
76	3.3000	108.51	0.0960	37.000
77	3.1000	126.25	0.0890	52.200
78	3.0000	94.260	0.103	21.000
79	2.9000	59.172	0.130	16.400
80	2.8000	71.818	0.118	31.100
81	2.7000	110.80	0.0950	30.500
82	2.6000	37.638	0.163	25.800
83	2.5000	123.46	0.0900	53.600
84	2.3000	108.51	0.0960	42.800
85	2.0000	164.37	0.0780	35.300
86	2.0000	64.000	0.125	13.000
87	2.0000	96.117	0.102	7.6000
88	1.6000	53.279	0.137	11.700
89	1.6000	192.90	0.0720	19.400
90	1.5000	182.62	0.0740	47.200
91	31.500	45.043	0.149	113.90
92	30.900	73.051	0.117	214.60
93	30.400	57.392	0.132	89.250
94	30.300	51.020	0.140	194.70
95	30.200	40.058	0.158	78.800
96	30.100	27.701	0.190	122.60
97	29.800	36.290	0.166	98.300
98	29.200	81.162	0.111	198.20
99	29.000	40.058	0.158	160.80
100	28.600	53.279	0.137	96.800
101	28.500	56.532	0.133	129.20
102	28.400	92.456	0.104	139.00
103	28.000	58.272	0.131	277.50
104	25.900	59.172	0.130	73.200
105	25.400	85.734	0.108	106.00
106	16.900	27.127	0.192	26.400
107	16.400	76.947	0.114	76.500
108	1.5000	148.72	0.0820	30.400
109	1.2000	132.12	0.0870	25.800
110	1.2000	177.78	0.0750	12.900
111	1.1000	126.25	0.0890	13.200
112	1.1000	115.62	0.0930	15.400
113	1.0000	84.168	0.109	17.500
114	1.0000	75.614	0.115	19.100
115	0.90000	106.28	0.0970	17.400

116	0.60000	132.12	0.0870	8.8000
117	0.50000	145.16	0.0830	7.0000
118	0.40000	152.42	0.0810	13.400
119	0.40000	106.28	0.0970	12.700
120	0.30000	132.12	0.0870	5.1000
121	0.30000	138.41	0.0850	6.3000
122	0.20000	164.37	0.0780	11.700
123	0.10000	138.41	0.0850	3.7000

Table 6. Quadrature data versus cation exchange capacity. The bulk tortuosity is given by the product $F\,\phi$. Note that 1 cmol kg^{-1} = 1 meq /(100 g) = 963.2 C kg^{-1}.

Sample	σ" (10^{-4} S m^{-1})	CEC (C kg^{-1})	Bulk tortuosity $F\,\phi$
#3477 (1)	1.50	237.74	3.0
#3336A (1)	1.17	393.65	4.7
#3478 (1)	1.41	417.70	3.4
#101 (1)	2.14	531.40	3.4
#102 (1)	1.29	599.84	3.3
#CZ10 (1)	2.13	772.91	4.1
#3833A (1)	2.23	1154.1	3.1
#3126B (1)	4.76	1446.1	2.9
#3847A (1)	1.42	754.56	6.0
#3283A (1)	3.43	1245.8	3.6
#3885B (1)	1.27	1676.7	5.9
#3972E (1)	3.52	1546.7	4.1
#3258A (1)	3.69	2022.1	6.4
#3891A (1)	4.36	3325.2	7.5
#3308A (1)	10.8	5498.4	3.5
#3323F (1)	12.0	10145	4.1
#3324A (1)	9.53	6623	6.6
#3323E (1)	13.5	9802	4.2
#3324B (1)	10.6	7843	6.0
#3306F (1)	10.9	7123	8.2
S9 (2)	11.0	1350	2.0
S16 (2)	16.5	5105	2.9
S22 (2)	15.5	11,560	1.9
S14 (3)	12.0	5047	2.8
S20 (3)	12.0	4999	1.7
S18 (3)	16.0	7570	2.6
S5 (3)	10.0	8254	2.0
S12 (3)	13.0	6598	1.9
S7 (3)	40.0	4777	1.8
PS1 (4)	9.0	1830	8.5
B100 (5)	50.9	48,000	-
B80 (5)	47.2	38,400	-
B60 (5)	41.4	28,800	-
B20 (5)	30.3	9,600	-
E6 (6)	2.94	1125	4.3
E7(6)	2.47	741	3.2
E10 (6)	2.75	1763	3.8

E12 (6)	0.61	284	3.3
E14 (6)	0.78	498	2.7
E17 (6)	0.114	46	4.7
B2 (6)	0.18	74	3.0
B4 (6)	0.44	99	2.7
R1 (6)	1.27	307	6.9
R3 (6)	1.44	384	4.4
C1 (7)	0.24	29.9	2.4
RSL (8)	6.7	3660	1.2
VEG2RI-2 (9)	5.6	5490	2.7
VEC15-5 (9)	7.7	7995	2.6
HEC18-7 (9)	16.2	7494	2.4
SB1 (10)	10.0	1596	3.0
SB2 (10)	5.28	2949	4.5
SB3 (10)	5.55	3278	6.1
SB4 (10)	8.10	3501	5.4
SB5 (10)	4.05	4563	8.7
SB6 (10)	3.68	4273	8.9
SB7 (10)	3.07	3354	8.0

(1) *Vinegar and Waxman* [1984]. Shaly sands, CEC measured with the procedure reported in *Mortland and Mellor* [1954]. Quadrature conductivity measured at 30 Hz (25°C). Values given at 2 M NaCl.

(2) *Revil et al.* [2013a]. Saprolite, CEC determined from surface conductivity data.

(3) *Revil et al*. [2013b, c]. Saprolite, CEC measured using $BaCl_2$.

(4) This work. Portland sandstone, CEC from the clay mineralogy.

(5) Unpublished work (bentonite mix with sand, 100%, 80%, 60%, and 20% bentonite weight percentage). Measurements made at 0.1 S m^{-1} NaCl. The CEC of the pure bentonite has been measured with barite. The CEC of the mixes is obtained from the CEC of the pure bentonite and the mass fraction of bentonite. The quadrature conductivity is given at 1 kHz because of the small size of the pores.

(6) *Börner* [1992] (sandstones σ_w = 0.1-0.2 S m^{-1} NaCl). The CEC values are obtained from the specific surface areas using $\mathrm{CEC} = Q_s S_{Sp}$ with Q_s = 0.32 C m^{-2} (see *Revil* [2012]).

(7) *Grunat at al*. [2013]. Haven loam soil. CEC using $BaCl_2$. σ_w = 0.1-0.2 S m^{-1} $CaCl_2$.

(8) *Schwartz et al*. [2014] and *Shefer et al*. [2013]. Red sandy loam. CEC using $BaCl_2$. σ_w = 0.12 S m^{-1}. 3 Hz.

(9) Sherwood sandstones, this work. 0.01 M NaCl. The CEC is obtained using ammonium.

(10) St Bees sandstone. Source: Mejus, L. (2014), Using multiple geophysical techniques for improved assessment of aquifer vulnerability, Unpublished PhD thesis, Lancaster University, Lancaster, UK. Salinity: 0.01 M NaCl. The CEC is obtained using ammonium.

Table 7. Quadrature data versus Grain diameter for natural and pure sands and glass beads. For silica grains, the equivalent CEC is given by CEC = 6 Q_S / (ρ_s d) with a surface charge density of Q_S = 0.64 C m^{-2}, d is the diameter of the sand grains, and ρ_s = 2650 kg m^{-3} denotes the mass density of the silica grains. The values of the quadrature conductivity are generally reported at their peak frequency.

Sample	σ" (10^{-4} S m^{-1})	d (μm)	CEC (C kg^{-1})	Bulk tortuosity $F\ \phi$
Z16X (1)	0.028	250	5.80	2.7
S#70 (2)	0.79	200	7.25	1.5
B#30 (3)	0.14	500	2.90	1.5
A#70 (3)	0.12	200	7.25	1.5
L1 (4)	0.020	260	5.57	1.6
F1 (5)	0.030	250	5.80	2.7
F3 (5)	0.018	250	5.80	8.0
U30 (6)	0.30	175	8.28	1.5
Sand B (6)	0.28	350	4.14	1.2
F36 (7)	0.0095	180	8.05	1.8
F32 (7)	0.0045	270	5.37	1.6
WQ1 (7)	0.0085	660	2.20	1.5
SP1 (7)	0.0060	180	8.05	1.5
SP2 (7)	0.0060	240	6.04	1.7
SP3 (7)	0.0070	320	4.53	1.6
SP4 (7)	0.0065	500	2.90	1.5
SP5 (7)	0.0150	680	2.13	1.5
SP6 (7)	0.0075	870	1.67	1.6
Ga38 (8)	0.060	100	14.5	1.4
G39 (9)	0.035	100	14.5	1.5
S1 (10)	0.023	180	8.05	1.5
S2 (10)	0.030	35	41.4	1.5
S1 (11)	1.05	168	8.63	1.3
B1-2 (12)	0.0843	1560	0.929	-
B2-2 (12)	0.0347	1910	0.759	-
B3-4 (12)	0.0900	1810	0.801	-
B4-1 (12)	0.0977	1870	0.775	-
B6-1 (12)	0.174	1180	1.23	-
C1-2 (12)	0.127	1010	1.43	-
C2-2 (12)	0.0836	1910	0.759	-
C3-2 (12)	0.0956	1590	0.911	-
C3-4 (12)	0.106	890	1.63	-
C4-5 (12)	0.171	730	1.99	-
C5-2 (12)	0.100	1970	0.736	-
C5-5 (12)	0.127	810	1.79	-

S1 (13)	0.03	200	7.25	1.4
Sand (14)	0.01	200	7.25	1.4

(1) *Revil et al*. [2014]. Fontainebleau sandstone. NaCl. 0.8 Hz.
(2) Unpublished (clean silica sand). 1 Hz. σ_w = 0.1 S m^{-1} NaCl.
(3) *Schmutz et al*. [2010]. 0.05 Hz. σ_w = 1.4×10^{-2} S m^{-1} NaCl
(4) *Slater and Lesmes* [2002]. 1 Hz.
(5) *Börner* [1992]. σ_w = 0.1 S m^{-1} NaCl.
(6) *Revil and Skold* [2011].
(7) *Koch et al.* [2011, 2012]. Natural sands. σ_w = 0.1 S m^{-1} NaCl.
(8) *Schmutz et al*. [2012]. Fontainebleau sand. σ_w = 0.039 S m^{-1} tap water.
(9) *Vaudelet et al*. [2011a]. Fontainebleau sand. σ_w = 0.03 S m^{-1} NaCl.
(10) *Leroy et al*. [2008]. Glass beads. σ_w = 0.005-0.041 S m^{-1}.
(11) *Joseph et al.* [2015]. Silica sand. σ_w = 0.1 S m^{-1} KCl.
(12) *Slater et al*. [2014]. Matrix of unconsolidated sediment. σ_w = 0.02 S m^{-1} NaCl.
(13) *Abdel Aal et al*. [2013]. Sand. σ_w = 0.1 S m^{-1} (artificial ground water). 10 Hz.
(14) *Breede et al*. [2012]. Sand. 1 Hz.

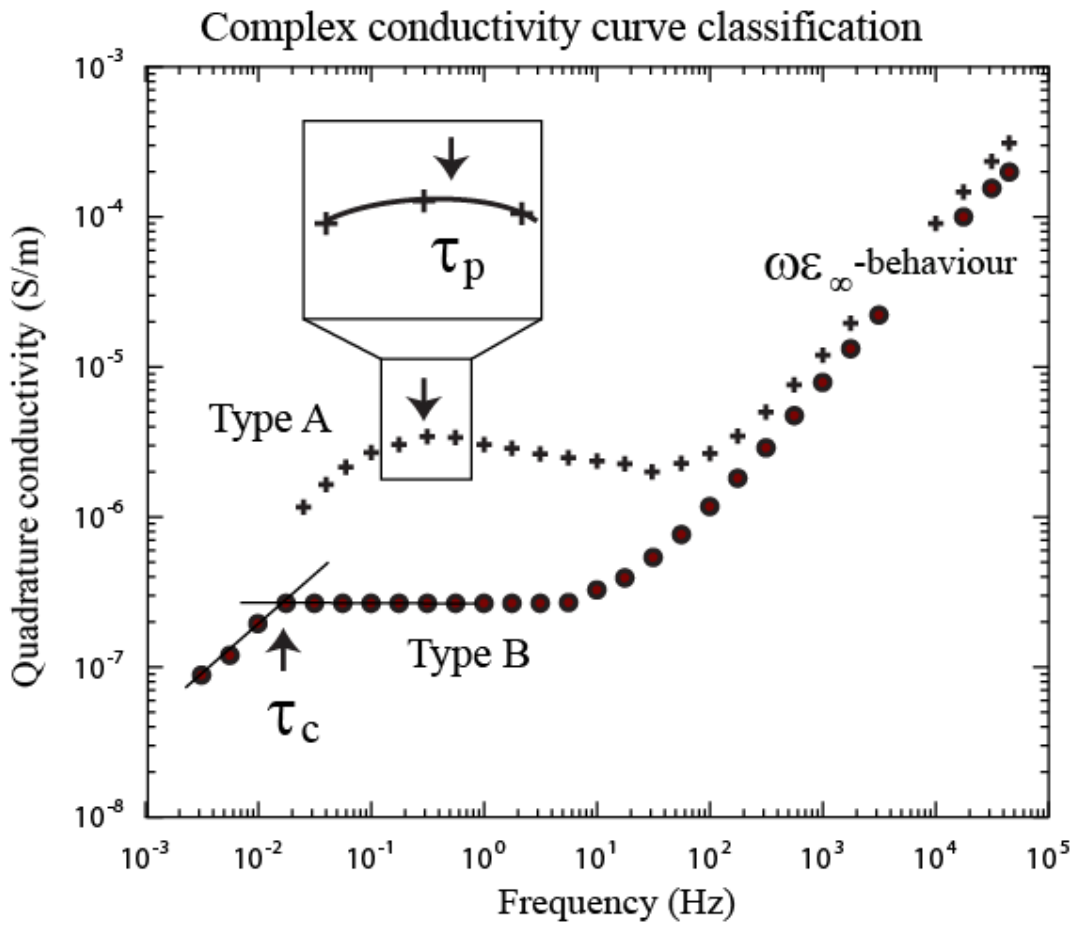

Figure 1. Classification of the absolute value of the quadrature conductivity curves. At low-frequency, we observe either a well-defined polarization peak (Type A) or a plateau (Type B). In the first case, the characteristic relaxation time is taken as the inverse peak frequency, which can be obtained through a polynomial fit of some data points and then looking for the inflexion point of the polynomial function. In the second case, we pick the characteristic "corner" frequency at which the quadrature conductivity starts to decrease rapidly towards zero (typically with a frequency dependence as $f^{-1/2}$), and consider its inverse as the characteristic relaxation time. This involves fitting the plateau and the low-frequency decay with two straight lines and looking for the cross-point of the two lines in a bilogarithmic plot. In both cases, the characteristic frequency is indicated by the vertical arrow. In both cases, the uncertainty in the quadrature conductivity measurements can be used to assess the uncertainty regarding the relaxation time. The parameters τ_c and τ_p denote the corner relaxation time and the peak relaxation time, respectively.

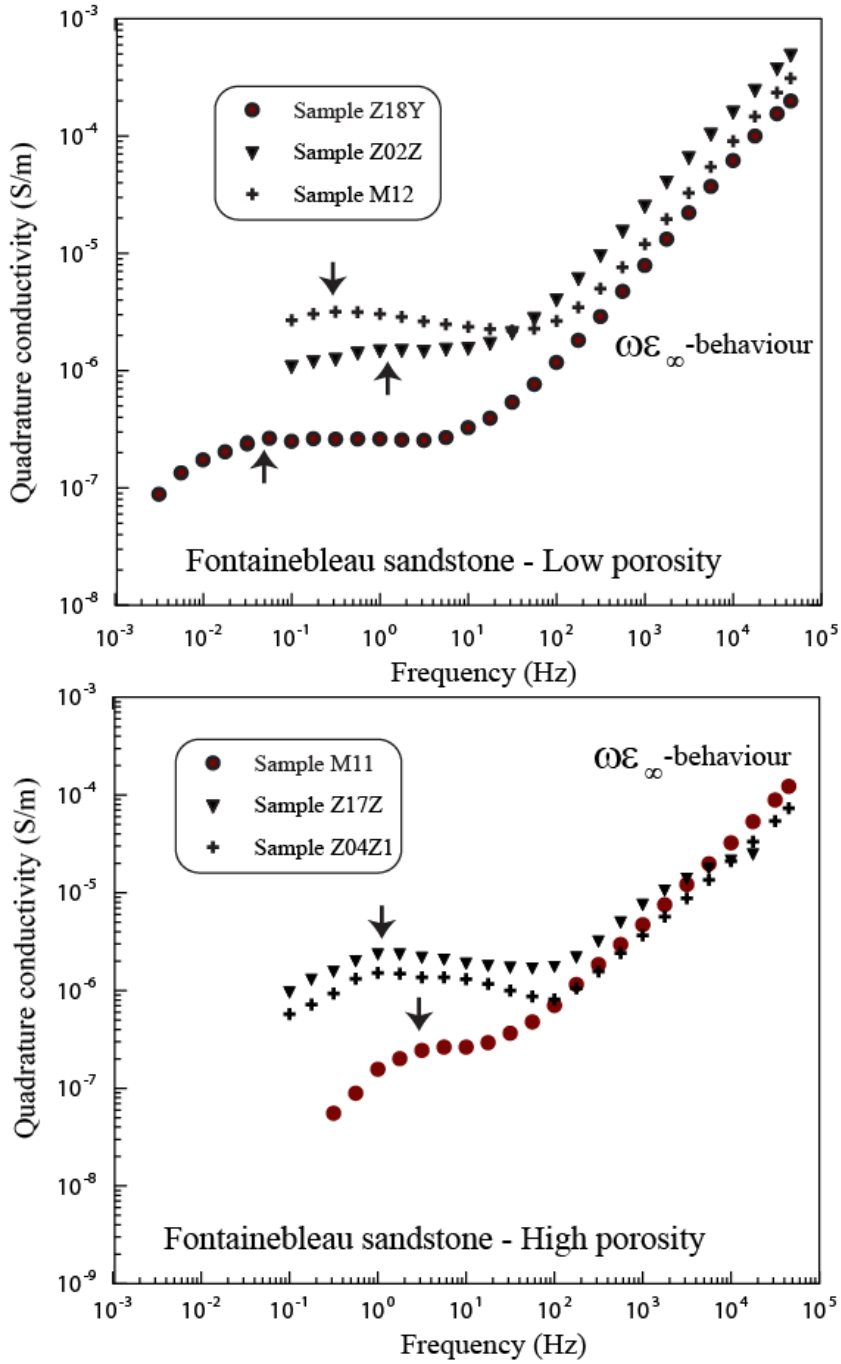

Figure 2. Left side: Typical spectra for the absolute value of the quadrature conductivity for the high and low porosity Fontainebleau sandstones. The arrows show the position of the characteristic frequency taken to predict the permeability. The $\omega\varepsilon_\infty$-behavior at high frequencies corresponds to the Maxwell-Wagner polarization and should not be misled with potential electromagnetic inductive and capacitive coupling effects. Measurements above 1 mHz with an uncertainty higher than 10% (computed on three cycles) and with a phase below the apparatus sensitivity (0.1 mrad below 100 Hz) are not shown. Data shown for a pore water conductivity of 165 μS cm^{-1} and a pH of 7.2.

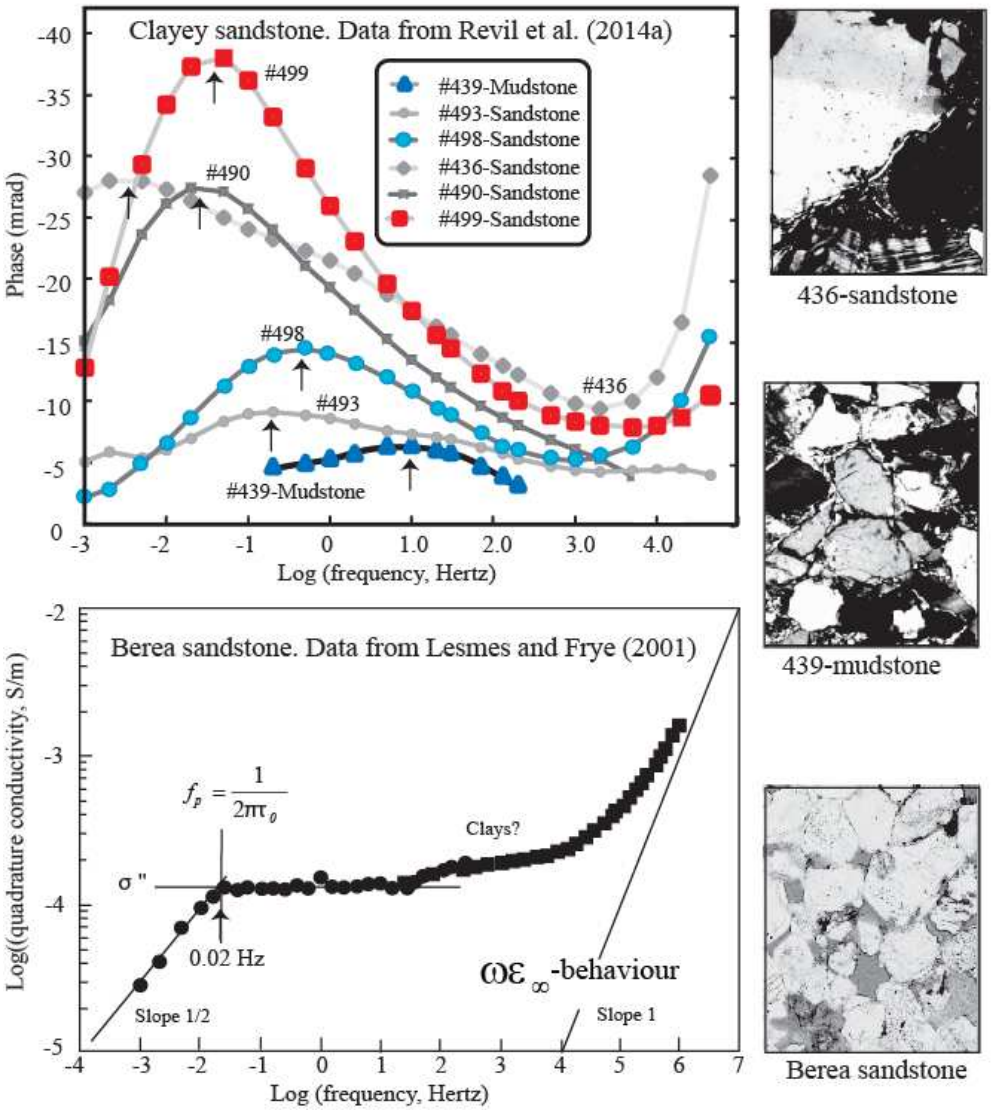

Figure 3. Typical examples of Type A (clayey sandstones from *Revil et al*. [2014a]) and Type B spectra (Berea sandstone from *Lesmes and Frye* [2001]). The Berea sandstone is a sandstone with a relatively minor clay content. The filled circles and squares correspond to the measurements with two distinct acquisition protocols. The arrows show the position of the characteristic frequency used to predict the permeability. The size of the thin section images is 1 mm in *x*. Uncertainty on the measurements is typically around 5% at low frequencies and 1 % or less at high frequencies. High frequencies (>100 Hz) can be contaminated with electromagnetic coupling effects. The logarithm is taken for the abolsute value of the quadrature conductivity.

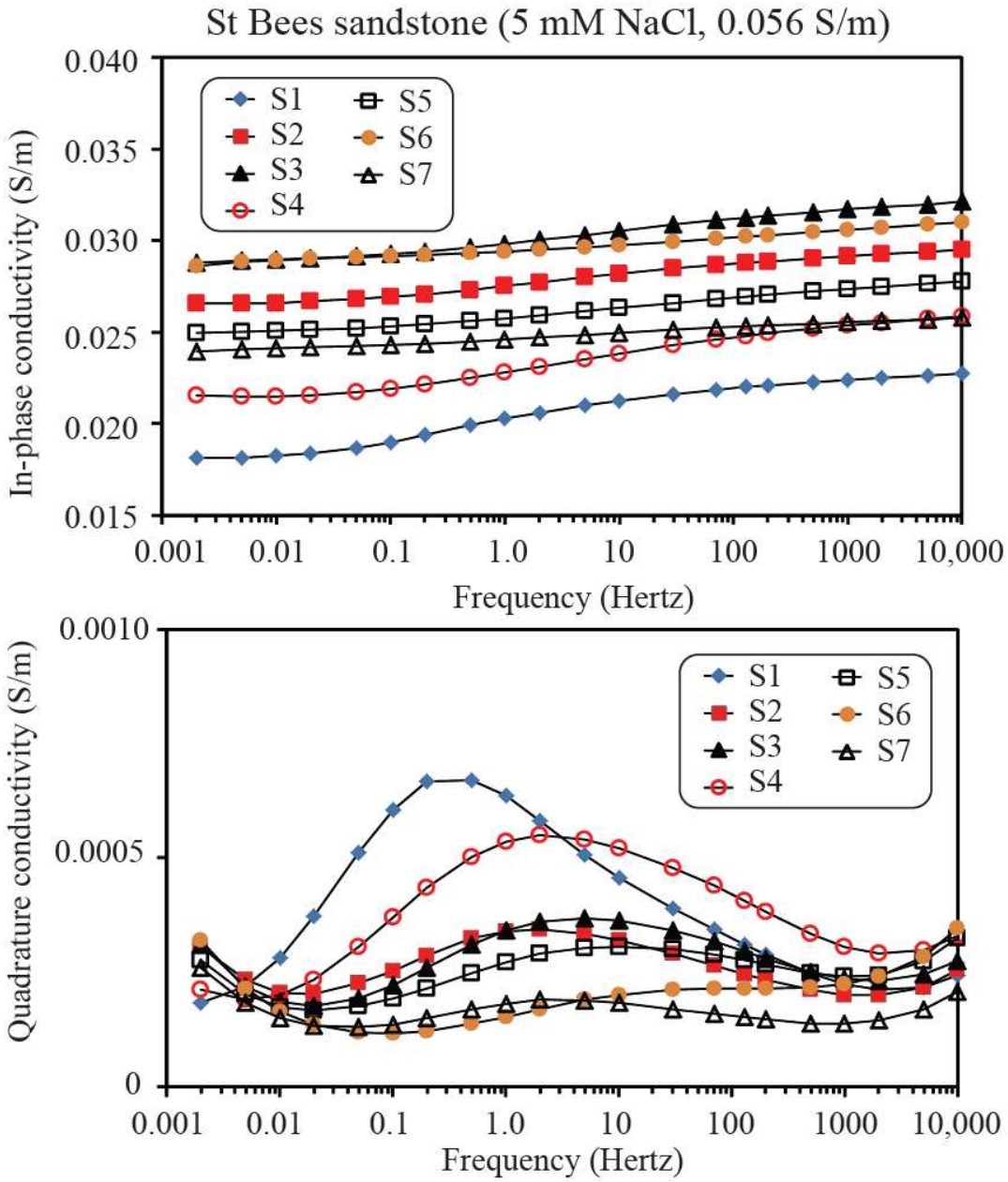

Figure 4. Absolute value of the quadrature conductivity spectra for the 7 samples of the St Bees sandstone from UK used in this study (see Table 2, 5 mM NaCl, conductivity: 0.056 S m^{-1} at 25°C). The core sample were obtained from the same core. Note that in the frequency range 0.01 Hz to 1 kHz, the quadrature conductivity spectra are characterized by a clear peak frequency, which is the characteristic frequency used in our prediction of the permeability.

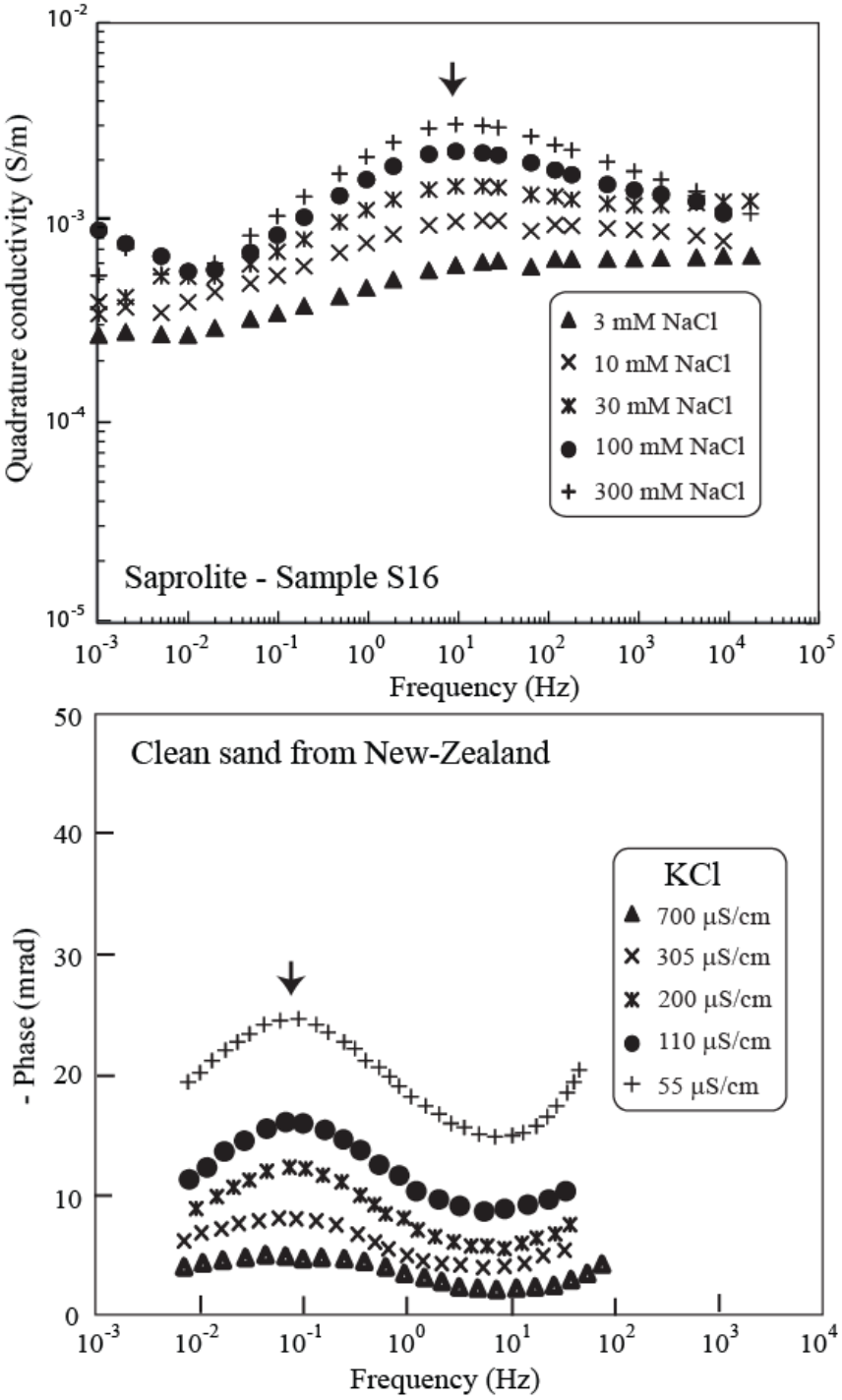

Figure 5. Influence of salinity upon the peak frequency. **a.** Quadrature conductivity spectra of a saprolite core sample at 5 different salinities (NaCl) showing how the peak relaxation time is poorly dependent on the salinity of the pore water. The peak frequency is shown by the arrow. **b.** Phase for a clean sand from New-Zealand (Sample 1, data from *Joseph et al*. [2015], reproduced with the permission of the authors). The sand is saturated by KCl solutions at different salinities. The peak frequency is shown by the arrow.

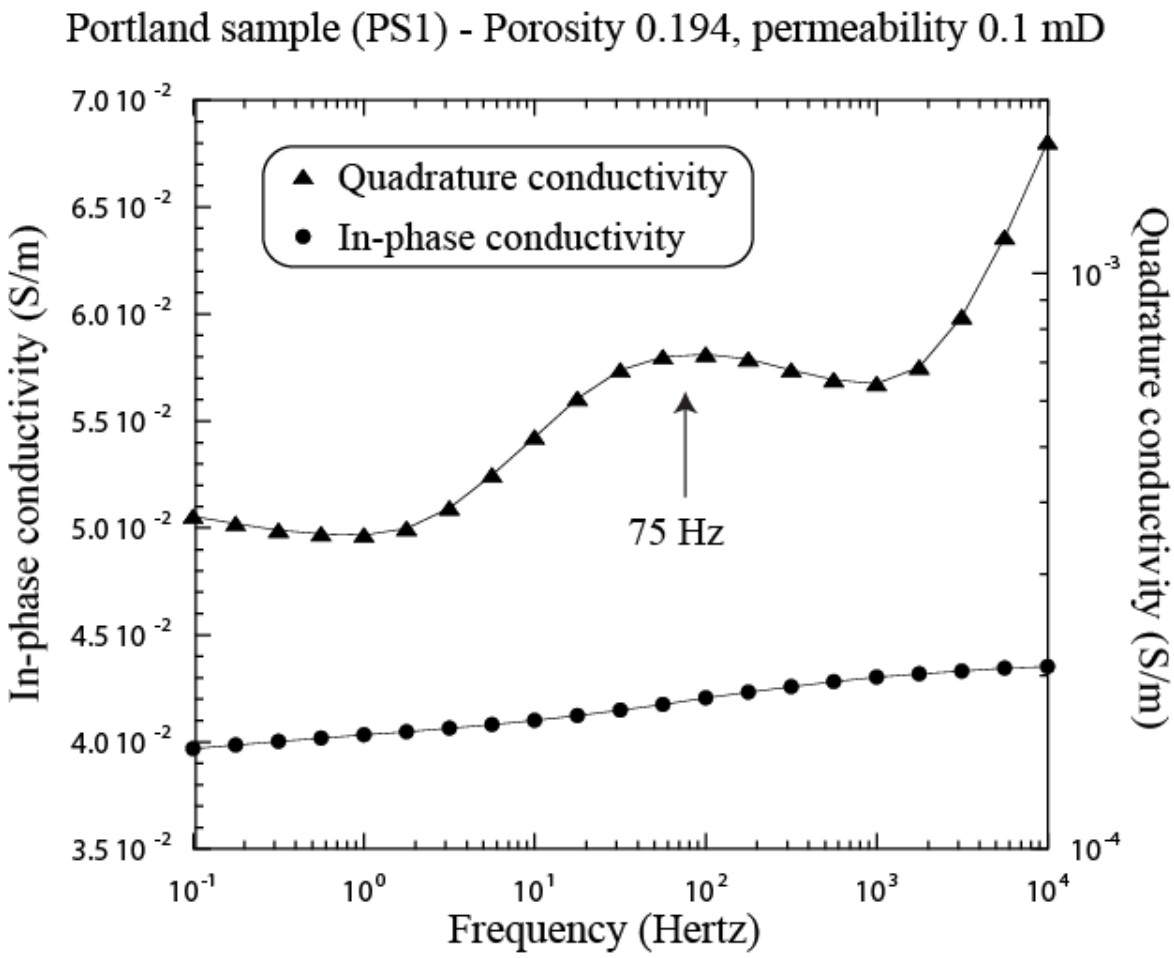

Figure 6. Complex conductivity spectrum for the Portland sandstone (an illite-rich sandstone) investigated in this study (Sample PS1). The pH was 9.1 and the conductivity of the pore water was 1.70×10^{-2} S m^{-1} (NaCl). The normalized chargeability M_n is $(4\pm1)\times10^{-3}$ S m^{-1}. The peak frequency used to predict permeability is shown by the arrow.

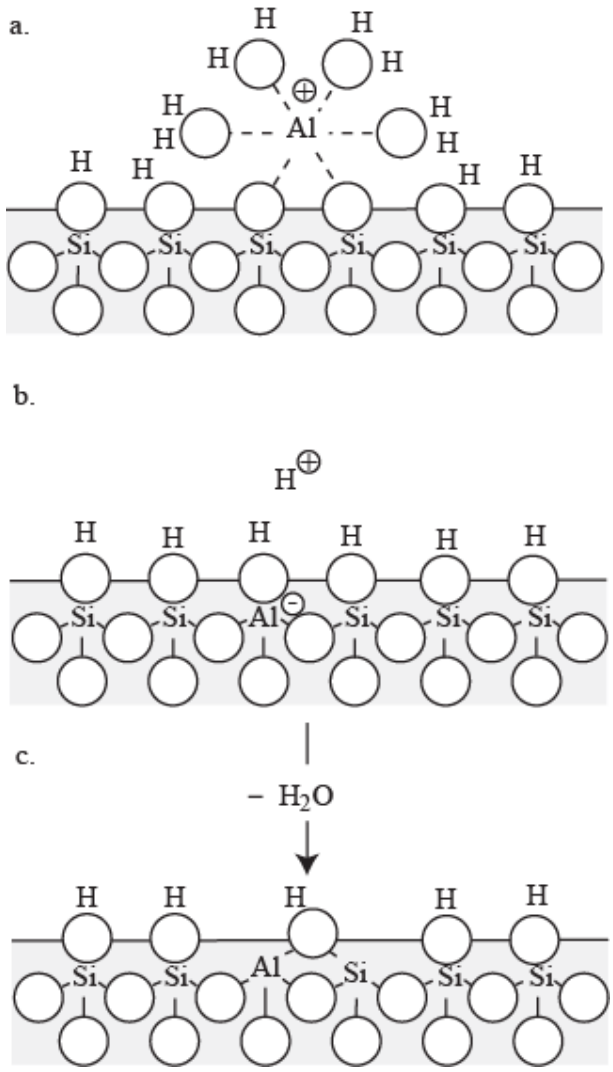

Figure 7. Incorporation of alumina through the surface of a clean sandstone like the Fontainebleau sandstone. **a.** Surface complexation on the mineral surface of a hydrated alumina cation. **b.** Incorporation of the alumina into the crystalline framework. **c.** After the assimilation of alumina, the surface of the sandstone possesses both aluminol and silanol surface sites. Its electrochemical properties can therefore differ from that of pure silica. The cement present in the Fontainebleau sandstone possesses alumina and its surface properties seem affected by its presence.

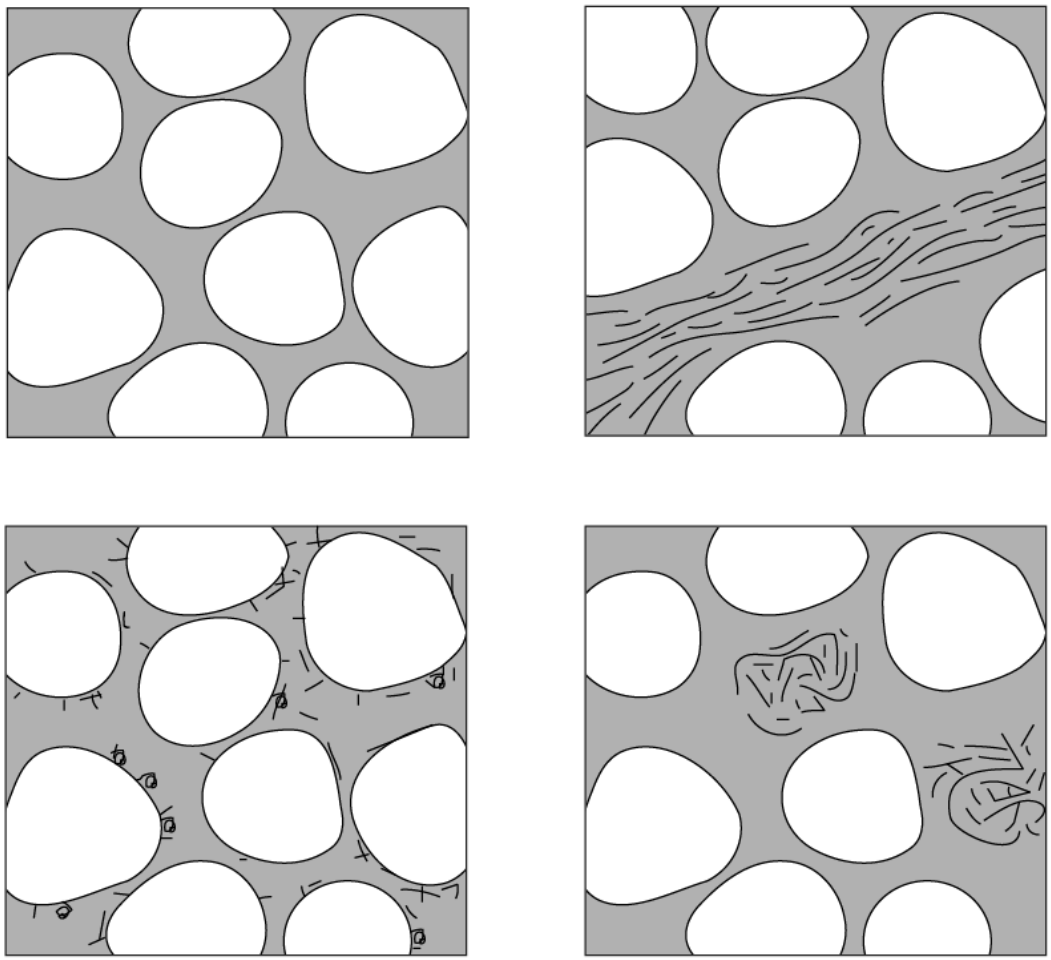

Figure 8. Classical clay-type distributions in sandstones. We expect our model to work for the clean sand and the case of dispersed clays coating the surface of the silica grains. In the case of the laminar shale and structural shale, the polarization is not expected to provide information regarding the pore size controlling the permeability of the material.

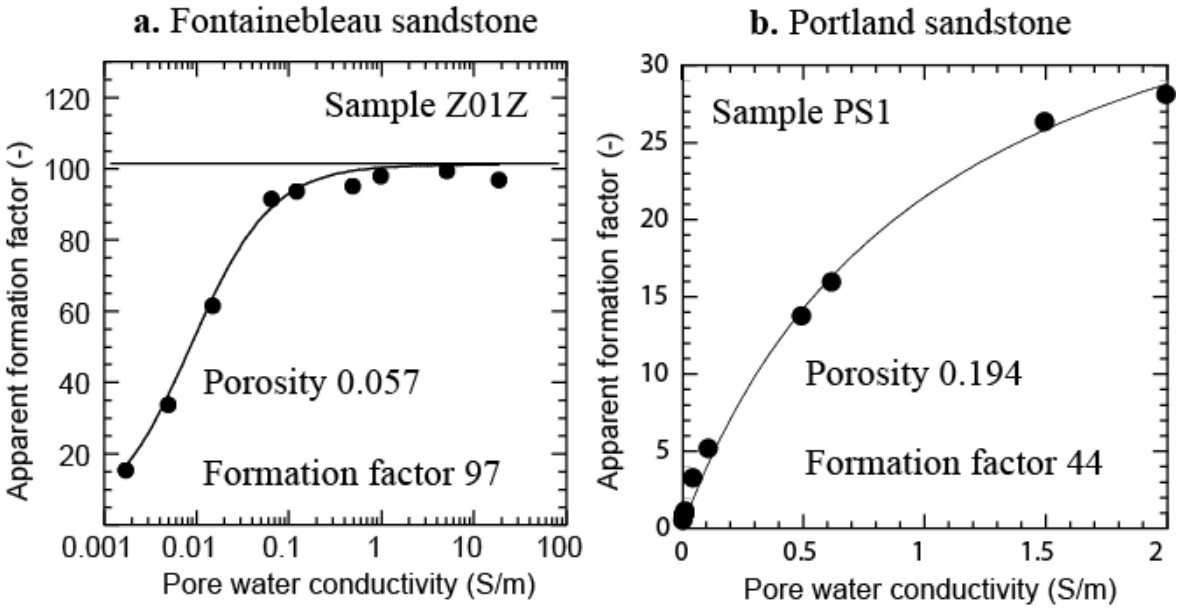

Figure 9. Apparent formation factor versus pore water conductivity for two of the samples in the database. The apparent formation factor is defined as the ratio of the conductivity of the pore water divided by the conductivity of the core sample. **a.** For the Fontainebleau sandstone (sample Z01Z, low porosity). The plain line denotes the linear conductivity model discussed in the main text. There is a strong difference between the apparent formation factor (which is not a textural property of the porous material) and the intrinsic one for clean sandstones except at very high salinities. Note that two additional salinities have been made with respect to the dataset used in *Revil et al*. [2014b]. **b.** Same for the Portland sandstone, a clay-rich sample. For this sandstone, the apparent formation factor is different from the (intrinsic) formation factor F even at 2 S m^{-1} for the conductivity of the pore water. The (inrinsic) formation factor is F = 43.8 ± 2.2 (and therefore m =2.3) while the surface conductivity (defined by Eq. 11) is σ_S = 0.024±0.002 S m^{-1}.

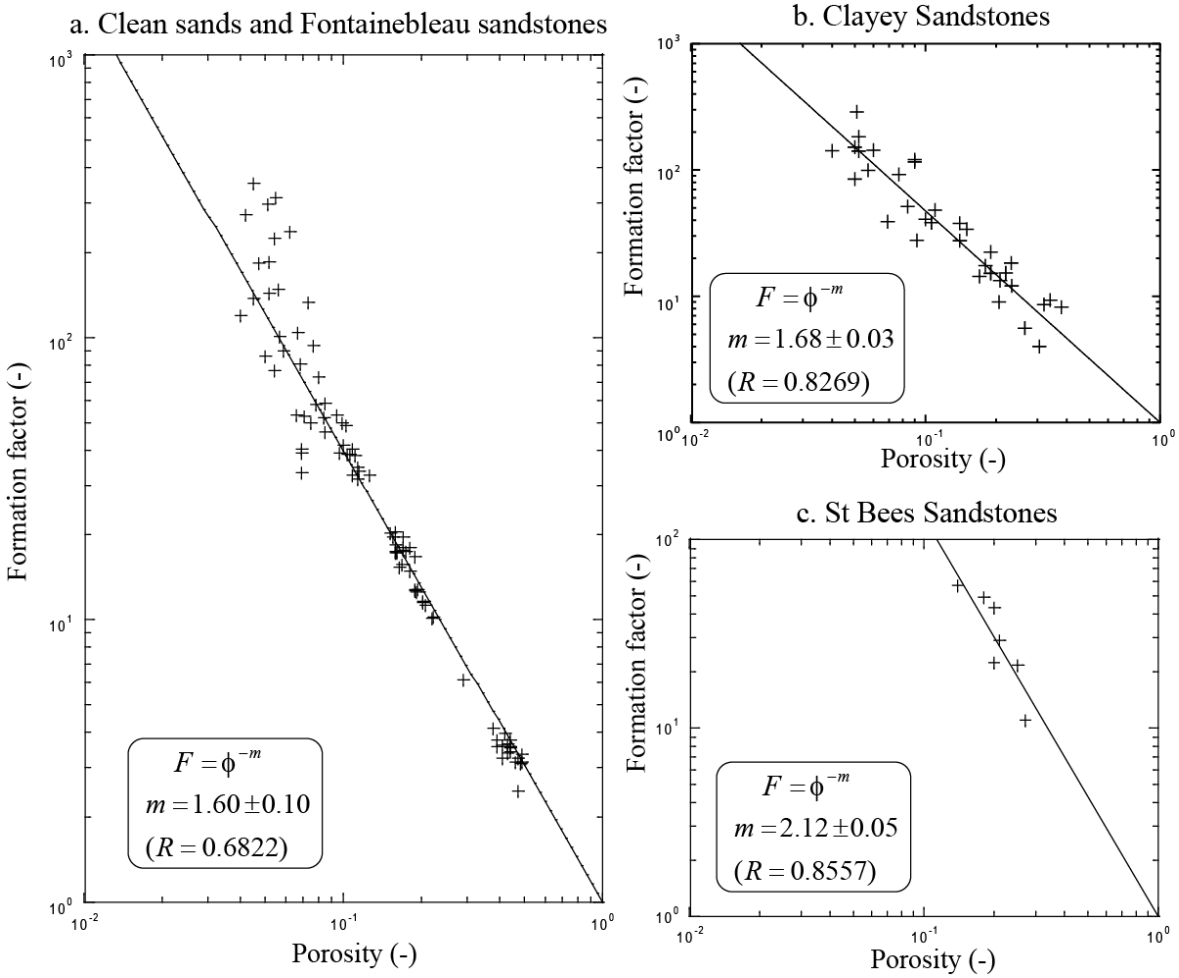

Figure 10. Test of Archie's law $F = \phi^{-m}$ for the clean sands and sandstones. **a.** Clean sands and Fontainebleau sandstones (Table 1 and *Revil et al*. [2014b]). **b.** Clayey sandstones (Tables 2 and 4 with the exception of the St Bees sandstone. **c.** St Bees sandstones (Table 2). In absence of measurements of the (intrinsic) formation factor, we can compute its value from porosity using a cementation exponent of 1.5 for clean sands and sandstones and 1.7 for clayey sandstones.

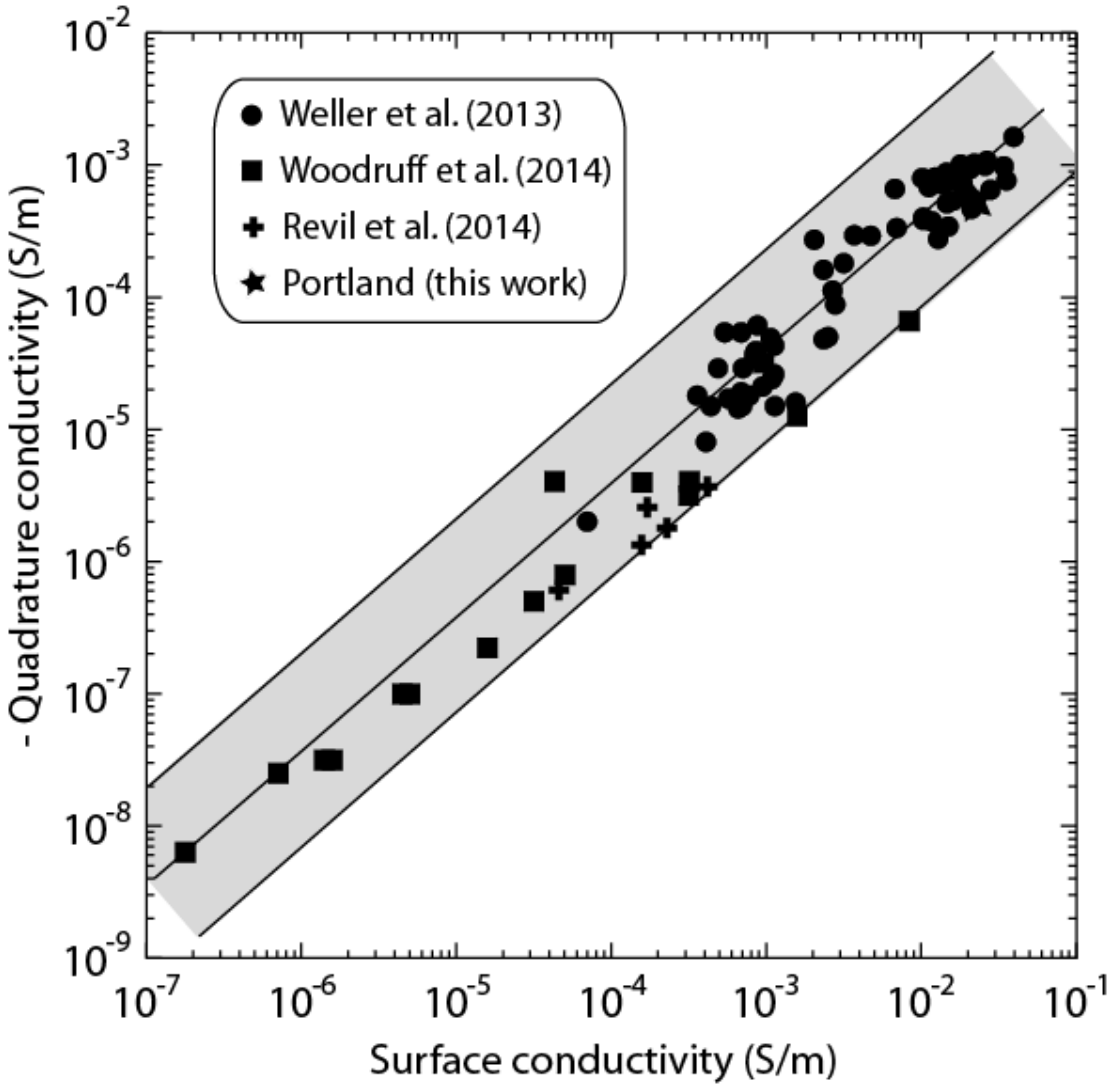

Figure 11. Absolute value of the quadrature conductivity versus surface conductivity for siliclastc materials. Data from *Weller et al*. [2013] for sands and sandstones, *Woodruff et al*. [2014] (oil and gas shales), and *Revil et al*. [2014] (Fontainebleau sandstones). The black lines corresponds to $-\sigma''/\sigma_S = 0.037\pm0.02$ (correlation coefficient $r^2 = 0.79$). This relationship is independent on the water saturation of the material and anisotropy. The grey area corresponds to the 98% confidence interval.

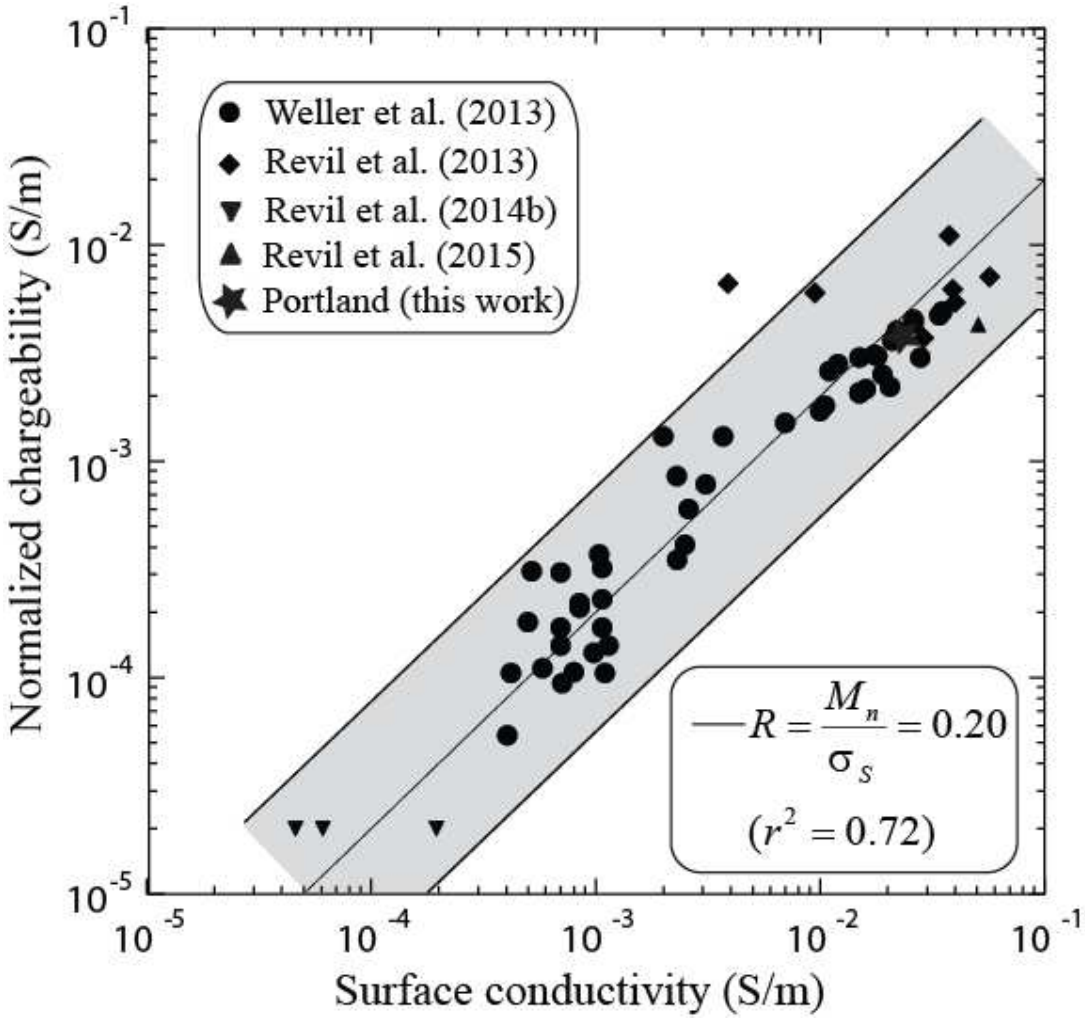

Figure 12. Normalized chargeability versus surface conductivity using the database of *Weller et al.* [2013] and a dataset including clean sandstones, clayey sandstones, and saprolites [see *Revil et al.*, 2013, *Revil et al.*, 2014b, and this work]. The grey area corresponds to the 98% confidence interval.

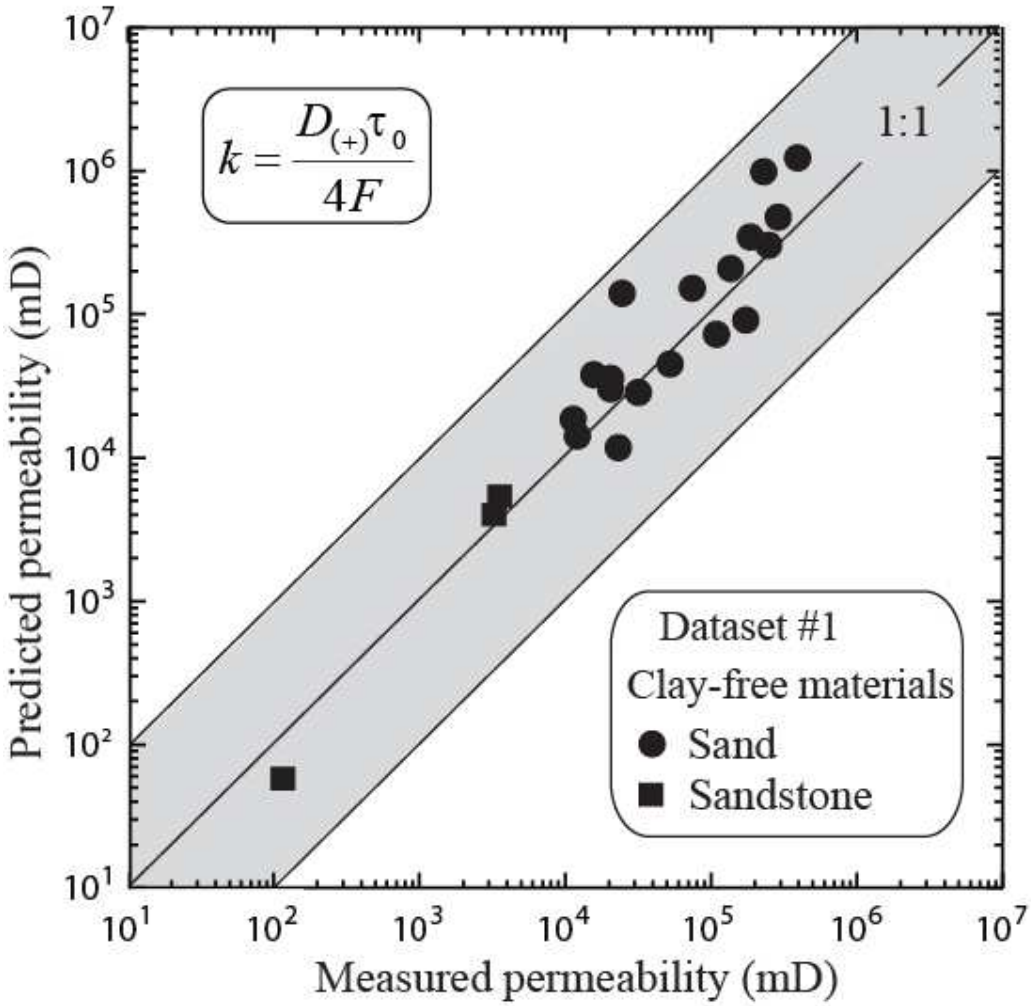

Figure 13. Predicted versus measured permeability (in mD) for the clean sand samples and the three high-porosity Fontainebleau sandstones (data from Table 1). We use $D_{(+)}(Na^+, 25°C) = 1.3 \times 10^{-9}\ m^2s^{-1}$, which is the value discussed in the text for pure silica. The grey area corresponds to plus or minus an order of magnitude for the prediction of the permeability. The dataset spans over four orders of magnitude.

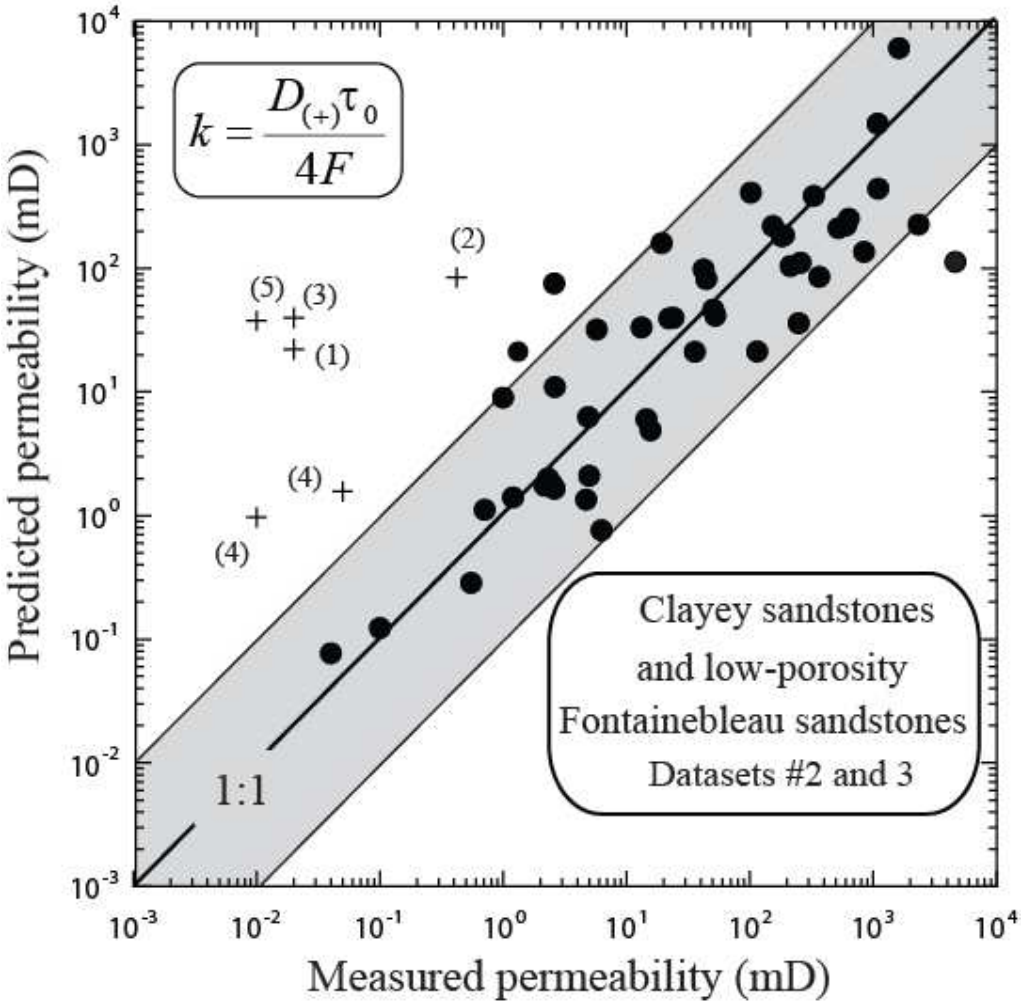

Figure 14. Predicted versus measured permeability (in mD) for the 53 clayey sandstones and low-porosity Fontainebleau sandstones (data from Tables 2 and 4). We use $D_{(+)}(Na^+, 25°C) = 3.8 \times 10^{-12}$ m^2s^{-1}, which is the value discussed in the main text for clay minerals. The 6 samples not following the trend are marked with a "+". They correspond to the following core samples (1) Sample Bu3 (Table 2), (2) Portland sample from *Titov et al*. [2010] (Table 2), (3) Samples 2T Tennessee sandstone (Table 4), (4) Samples AC2 and AC4 Arizona Chocolate (Table 4), (5) Sample 5T Tennessee sandstone (Table 4). The grey area corresponds to plus or minus an order of magnitude with respect to the predicted trend. Note that the measured permeability of sample 5T and AC2 are likely to be less as they are close to the limit of the measurement.

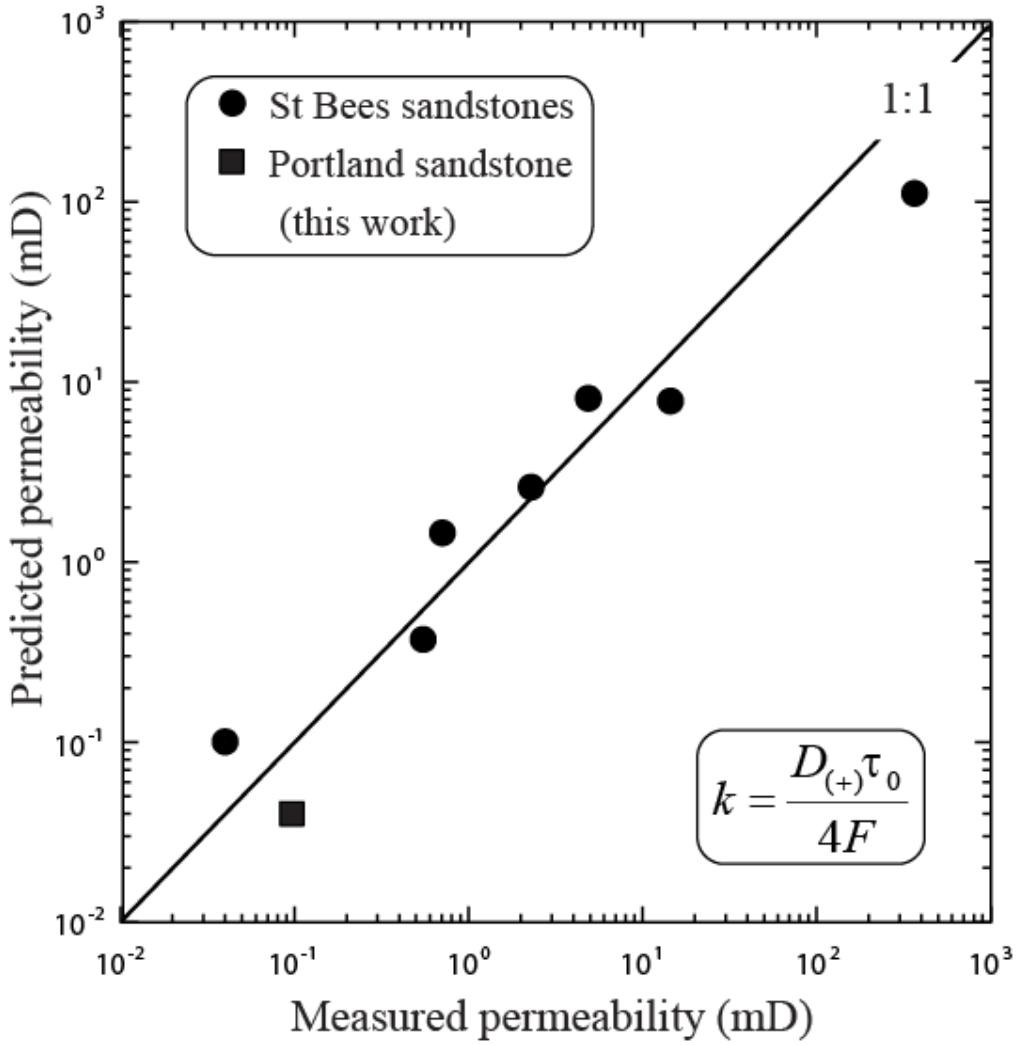

Figure 15. Predicted versus measured permeability (in mD). These new results are obtained for the clayey St Bees and Portland sandstones, both investigated in the present work. The data from the St Bee sandstones are from Table 2. The spectra of the St Bees sandstone samples are shown in Figure 4. The complex conductivity of the Portland sandstone (a very clayey sandstone) is shown in Figure 6. For both datasets, we use $D_{(+)}(Na^+, 25°C) = 3.8 \times 10^{-12}\ m^2s^{-1}$, which is the value recommended in the main text for clay minerals. Note that the predictions are here much better than plus or minus an order of magnitude.

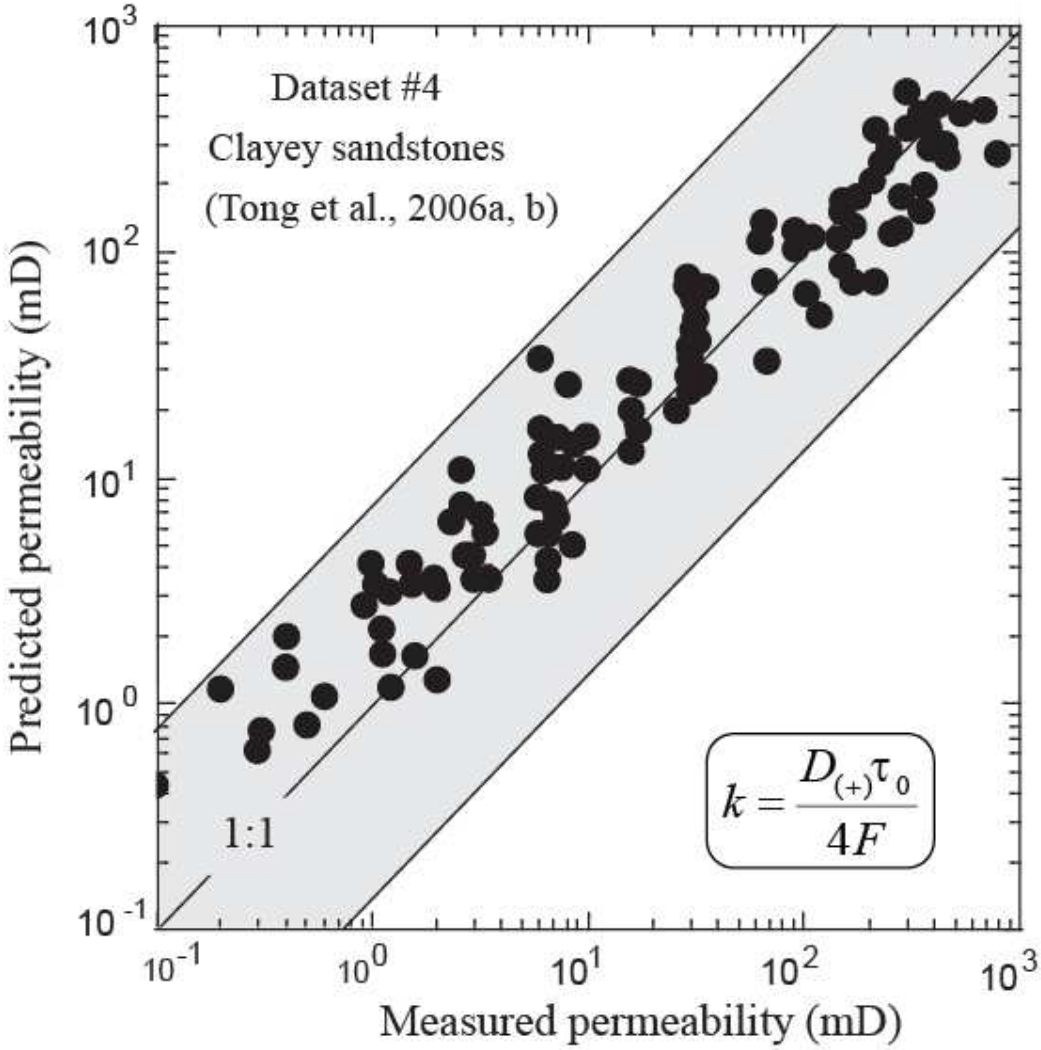

Figure 16. Predicted versus measured permeability (in mD) for the sandstones investigated by *Tong et al*. [2006a]. The relaxation time given by *Tong et al*. [2006a] and obtained from time-domain measurements needs to be multiplicated by a factor 17.1 to be compatible with the characteristic time constant determined in the frequency-domain according to the procedure described in Figure 1. This factor has not been fully justified and further work is needed to see how it can be explained form then definition adopted by *Tong et al*. [2006a] for their relaxation time. We use $D_{(+)}$ (Na^+, 25°C) = 3.8×10^{-12} m^2s^{-1}.

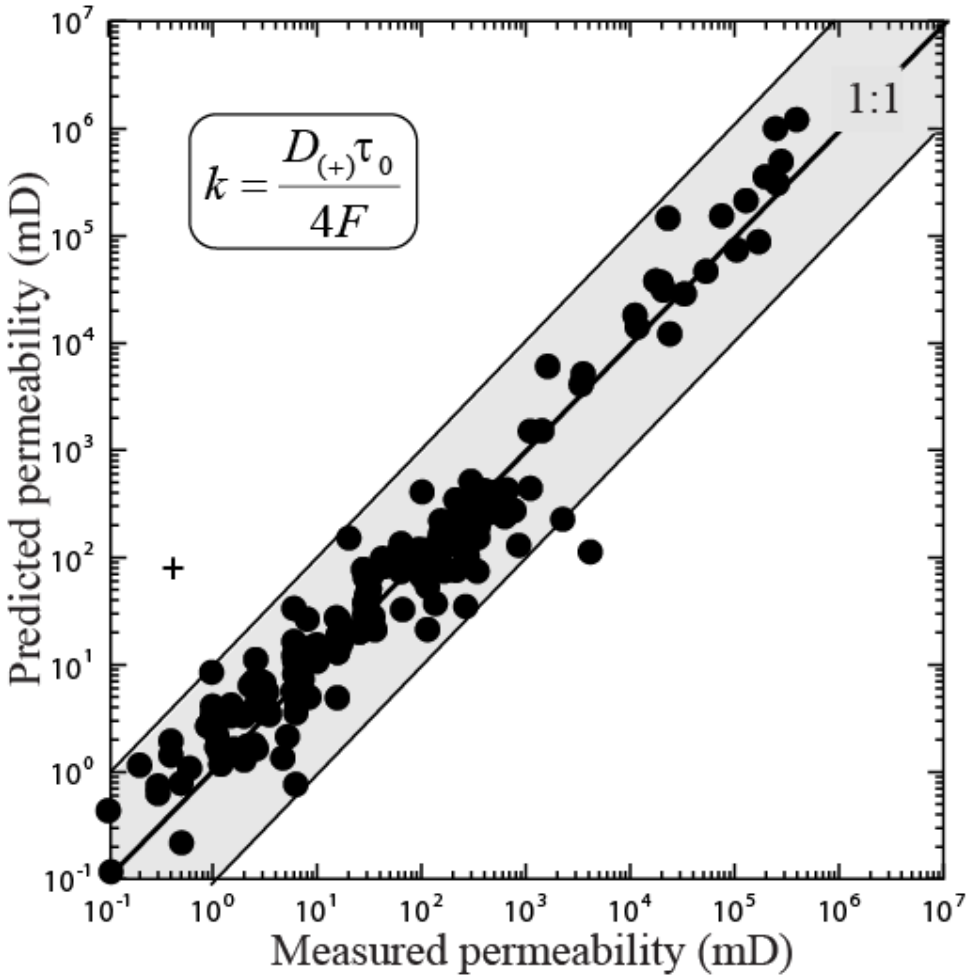

Figure 17. Predicted versus measured permeability for Datasets #1 to #4 (all the samples are shown with permeabilities higher than 0.1 mD). The shaded area corresponds to plus or minus one order of magnitude in the permeability determination. The only sample that is outside the trend (indicated by a plus sign) is the Portland core sample investigated by *Titov et al*. [2010] using time-domain induced polarization data. Our prediction seems reasonable over 7 orders of magnitude. The other outliers from Figure 14 do not appear in this figure since they correspond to permeability values below 0.1 mD. The model appears therefore reliable for permeabilities higher than 0.1 mD.

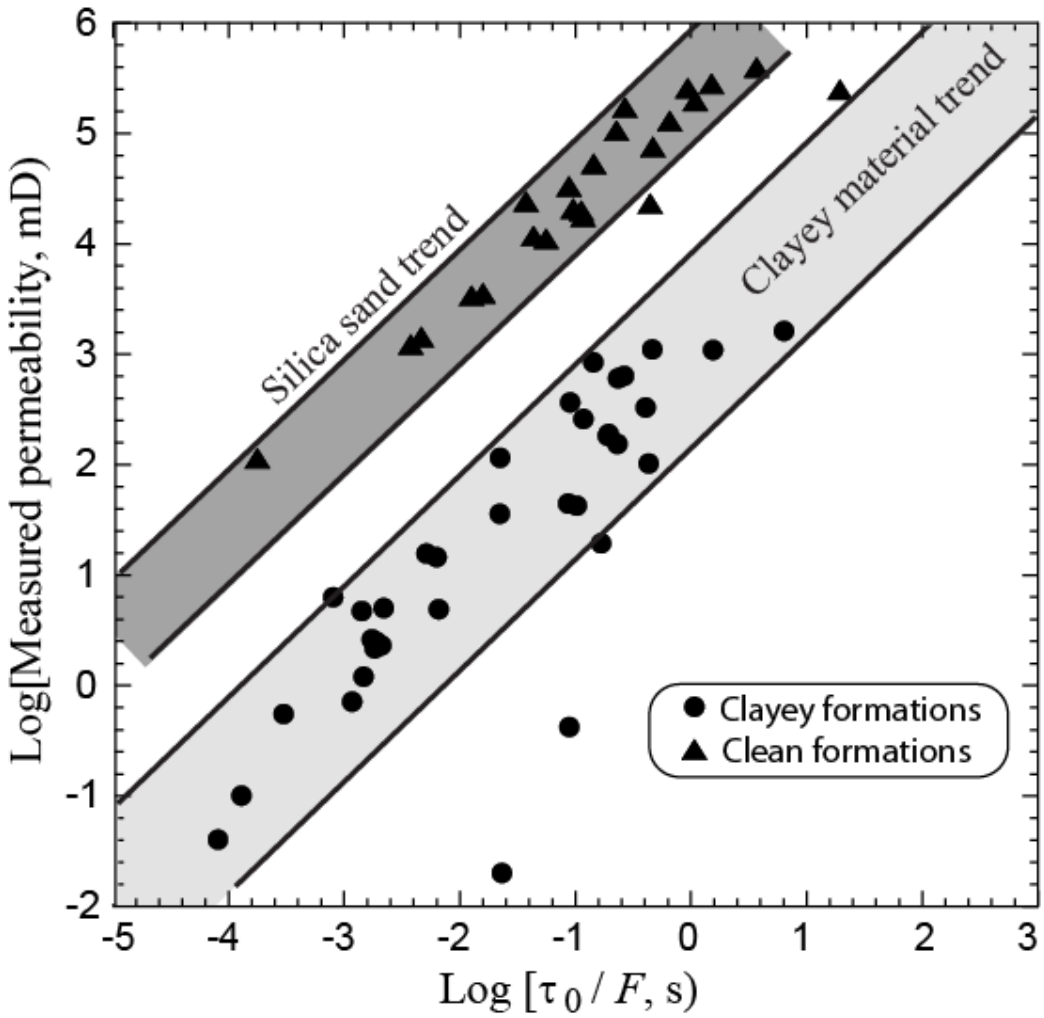

Figure 18. Permeability versus the ratio between the relaxation time and the intrinsic formation factor. Evidence for two discrete values of the diffusion coefficient for the counterions of the Stern layer associated with the properties of the mineral surface and not with the clay content per se. Permeability versus the ratio between the characteristic relaxation time and the intrinsic formation factor indicating the existence of two distinct values of the diffusion coefficients, one for perfectly clean silica sands and one for clayey formations. Datasets #1 and #2 (Tables 1 and 2).

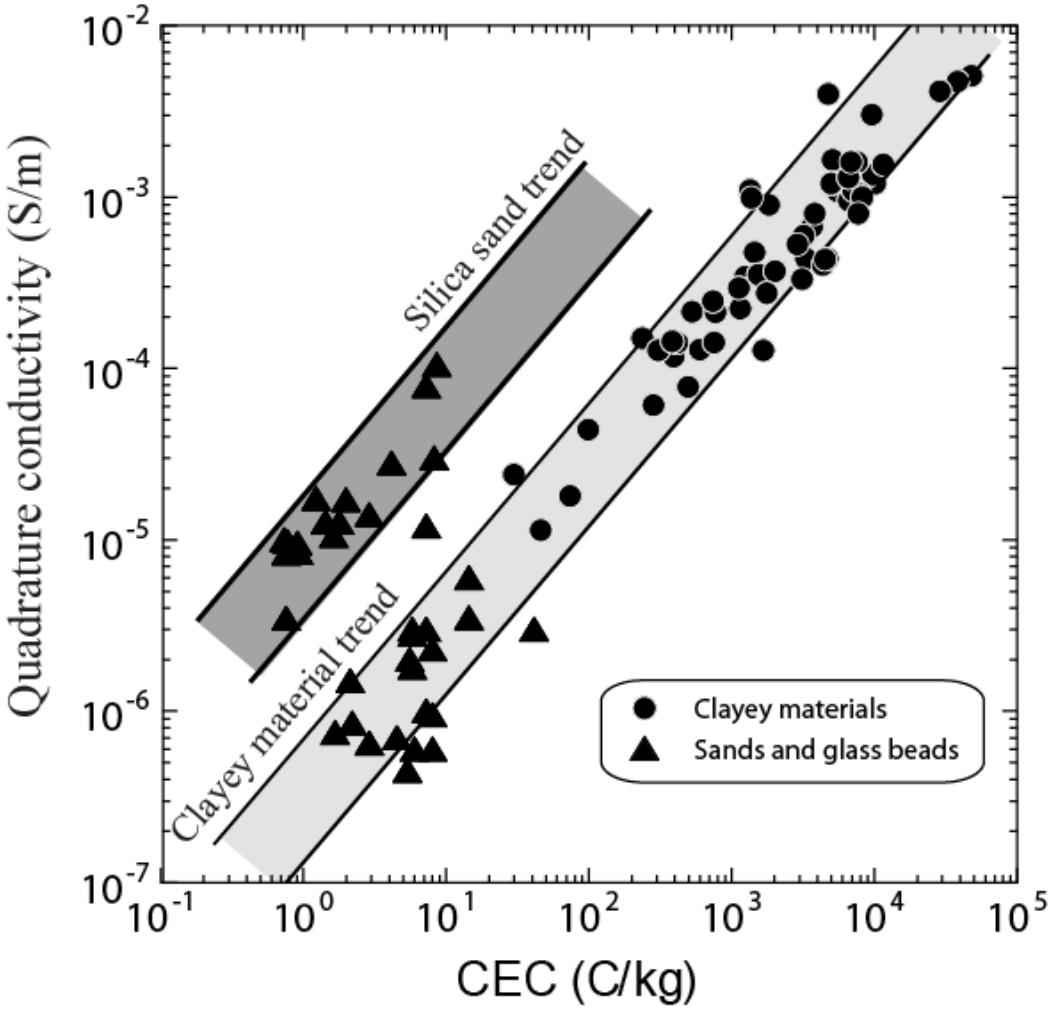

Figure 19. Quadrature conductivity versus cation exchange capacity. Evidence for two discrete values of the mobility for the counterions of the Stern layer associated with the properties of the mineral surface and not with the clay content per se. Quadrature conductivity versus CEC for clean sand clayey formations characterized by the same bulk tortuosity (see Tables 6 and 7 for the datasets). The permeability and quadrature conductivity data are mutually consistent in terms of relationship between the diffusion coefficient and the mobilities through the Nernst-Einstein relationship (compare Figures 18 and 19).